Synthesis of nickel-based catalysts and their application in pyrolysis oil upgrading in a batch reactor

María Belén Gagliardi Reolon

Master's degree in Energy Technologies - MSc ENTECH

Final thesis

Tutor: M. Sc. Ing. Caroline Carriel Schmitt (IKFT - KIT)

Correctors: Prof. Dr.-Ing. Martin Gabi (FSM - KIT), Dra. Ing. Cecilia Smoglie (ITBA)

Karlsruhe, 29th May 2018

Acknowledgments

I would like to thank Dr. Klaus Raffelt for the opportunity to carry out my master's thesis at the Institut für Katalyseforschung und -technologie (IKFT) and his friendly disposition to help when things did not go as expected.

I sincerely thank Caroline Carriel Schmitt, who was not only my tutor, but also a teacher and a friend. Thanks to her, these eight months of hard work were easy-going, amusing and full of great learning.

I would like to thank Pia Griesheimer, Jessica Heinrich, Birgit Rolli, Simon Wodarz, Oliver Schade, Kai Kalz, Michael Zimmermann, Christiane Altesleben, Roland Fritz, Thi-Bach-Cuc Ly, Bingfeng Guo, Sheng Wang and Yujie Fan for their technical assistance, measurements and helpful advice along these months.

Thanks to Dra. Cecilia Smoglie and Dr. Martin Gabi for the opportunity, full support and invaluable assistance during the entire master´s degree. This experience has definitely changed my life.

Special thanks to Paula Alfonso, Emmanuel Contreras Ordoñez, Patricio Costantini, Sebastián Oettinger, Joaquín Ortíz and Zeno Farina for their heart-warming friendship and long-lasting backing. You are the best group anyone could ever ask for.

Heartfelt thanks to William Fanet for his great encouragement, high motivation and support during the tough writing process.

Finally, I would like to thank my sister, my parents and my whole family for their constant presence, understanding, support and warm words of encouragement in my new german adventure. You are always on my mind.

I dedicate this work to my sister Vick, who showed me the right path when difficult times were ahead.

Declaration of authorship

I declare that I have developed and written the content of this master's thesis entirely by myself, and that I have not used unreferenced sources. Any thoughts from other authors or literal quotations are clearly marked. This work has not been used in the same or a similar version to achieve an academic grading or is being published elsewhere.

Abstract

English

The thermochemical decomposition of beech wood biomass results in a poor quality bio-oil, which cannot be directly used in diesel engines. In order to make this oil resemble liquid fossil fuels, an upgrading technique should be applied. Among the available possibilities, hydrodeoxygenation (the removal of oxygen and saturation of double bonds through high pressure hydrogen) appears to be the most auspicious route to produce biofuels. Besides, this method requires a catalyst to increase the activity, which could be reused in further upgrading reactions so as to minimize the generation of waste material.

In this work, four nickel-based catalysts were evaluated for the hydrodeoxygenation of beech wood bio-oil. After being synthesized, their superficial and compositional characteristics were assessed. Once the upgrading reaction was performed for the pyrolysis oil, the resulting products (upgraded bio-oil, aqueous phase and gas fraction) were separately analyzed. Considering the obtained results, the catalyst with the best upgrading performance was selected in order to regenerate and use it in further hydrodeoxygenation reactions. The catalyst selection was based on upgraded bio-oil, catalyst and reaction factors. Parameters such as carbon, oxygen and water content, HHV, pH value, poisoning and overall hydrogen consumption were taken into account.

With the obtained results, Ni/SiO_2 was chosen and therefore regenerated, which included the calcination and reduction of the spent catalyst before it was reused in a new hydrodeoxygenation reaction. Its performance was tested along three consecutive reactions and the quality of upgraded bio-oils corresponding to these cycles were evaluated. It could be concluded that Ni/SiO_2 showed an improvement in the upgraded bio-oil quality next to a satisfactory performance after the three regeneration cycles, which points out that this particular catalyst can be regenerated and reused for a minimum of three times without significantly affecting the resulting upgraded bio-oil quality. Further characterization techniques should be performed in order to achieve a bigger understanding of the functioning of nickel-based catalysts and their reutilization in a larger number of consecutive upgrading reactions.

Español

La descomposición termoquímica de la biomasa maderera de especies pertenecientes al género *Fagus* resulta en un bio-aceite de baja calidad que no puede ser usado directamente en motores diesel. Con el objetivo de que se asemeje a los combustibles fósiles, una técnica de mejoramiento debería ser aplicada. Entre las opciones disponibles, la hidrodeoxigenación (es decir, la remoción de oxígeno y saturación de dobles enlaces mediante hidrógeno a alta presión) parece ser el camino indicado para producir este tipo de biocombustibles. Además, este método requiere un catalizador para incrementar su actividad, que podría ser reutilizado en futuras reacciones de mejoramiento para minimizar así la generación de residuos.

En este trabajo, cuatro catalizadores a base de níquel fueron evaluados para la hidrodeoxigenación del bio-aceite de la madera de *Fagus*. Luego de la síntesis, se evaluaron las características superficiales y composicionales de los catalizadores. Después de realizar la reacción de mejoramiento para el bio-aceite, los productos resultantes (bio-aceite mejorado, fase acuosa y la fracción gaseosa) fueron analizados por separado. Considerando los resultados obtenidos, el catalizador con el mejor desempeño fue seleccionado con el objetivo de ser regenerado y reutilizado en futuras reacciones. La selección del catalizador se basó principalmente en factores relacionados con el bio-aceite mejorado, el catalizador y la reacción. Se tuvieron en cuenta parámetros como el contenido de carbono, oxígeno y agua, valor calorífico, pH, contaminación del catalizador y consumo de hidrógeno por parte de la reacción.

Con los resultados disponibles, se seleccionó y regeneró a Ni/SiO_2, lo que incluyó la calcinación y reducción del catalizador "gastado", con anterioridad a su reutilización en una nueva reacción de hidrodeoxigenación. Su desempeño y la calidad de los bio-aceites resultantes fueron evaluados a lo largo de tres reacciones consecutivas. Se pudo concluir que Ni/SiO_2 demostró un mejoramiento en la calidad del bio-aceite, además de un desempeño satisfactorio luego de las tres regeneraciones, lo que indica que este catalizador puede ser regenerado y reutilizado por un mínimo de tres veces sin ver afectada su actividad y la calidad del producto deseado. Nuevas técnicas de caracterización deberían ser utilizadas para poder lograr una mayor comprensión del funcionamiento de los catalizadores a base de níquel y su reutilización en un mayor número de reacciones de mejoramiento.

Deutsch

Der thermochemische Abbau von Buchenholzbiomasse führt zu einem minderwertigen Bioöl, welches nicht direkt in Dieselmotoren eingesetzt werden kann. Um jedoch mit den herkömmlichen fossilen Brennstoffen mithalten zu können, sollte eine Aufwertungstechnik angewendet werden. Unter den verfügbaren Möglichkeiten scheint die Hydrodeoxygenierung (die Entfernung von Sauerstoff und die Sättigung von Doppelbindungen durch Hochdruckwasserstoff) die vielversprechendste Variante zur Herstellung von Biokraftstoffen zu sein. Um die Aktivität der Hydrodeoxygenierung weiter zu erhöhen, wird ein Katalysator benötigt, welcher wiederverwendet werden kann, so dass Abfallmaterial minimiert werden kann.

In dieser Arbeit wurden vier Katalysatoren auf Nickelbasis für die Hydrodeoxygenierung von Buchenholz-Bioöl untersucht. Nach der Synthese wurden die oberflächlichen und kompositorischen Eigenschaften der Katalysatoren bewertet. Nachdem die Veredelungsreaktion für das Pyrolyseöl durchgeführt wurde, wurden die resultierenden Produkte (schwere Phase, leichte Phase und Gasfraktion) getrennt analysiert. Unter Berücksichtigung der Ergebnisse, wurde der Katalysator mit der besten Veredelungsleistung ausgewählt, welcher schließlich bei weiteren Hydrodeoxygenierungsreaktionen verwendet wurde. Die Katalysatorauswahl basierte dabei auf den verbesserten Bioöl-, Katalysator- und Reaktionsfaktoren. Parameter wie Kohlenstoff-, Sauerstoff- und Wassergehalt, HHV, pH-Wert, Vergiftung und der gesamte Wasserstoffverbrauch wurden berücksichtigt.

Die Ergebnisse ließen darauf schließen, dass Ni/SiO_2 die beste Veredelungsleistung generiert. Das Ni/SiO_2 wurde regeneriert, was die Kalzinierung und Reduktion des verbrauchten Katalysators beinhaltete, bevor der Katalysator erneut in einer neuen Hydrodeoxygenierungsreaktion verwendet wurde. Seine Leistung wurde in drei aufeinanderfolgenden Reaktionen getestet. Zudem wurde die Qualität der verbesserten Bioöle, die diesen Zyklen entsprachen, bewertet. Es konnte geschlussfolgert werden, dass Ni/SiO_2 eine Verbesserung der Bioölqualität nach den drei Regenerationszyklen zeigte. Dies ist ein Hinweis darauf, dass der getestete Katalysator mindestens dreimal regeneriert und wiederverwendet werden kann, ohne die daraus verbesserte Bioöl-Qualität signifikant zu beeinflussen. Zukünftig sollten weitere Charakterisierungstechniken durchgeführt werden, um ein besseres Verständnis der Funktionsweise von Katalysatoren auf Nickelbasis und deren Wiederverwendung in einer größeren Anzahl aufeinander folgender Aufwertungsreaktionen zu erreichen.

Index

1. Motivation

The steady increase in global energy demand in addition to pollution, climate change and the depletion of fossil fuel reserves have drawn attention to renewable energy sources, particularly to biomass[1–3]. This is mainly due to its low prices, widespread availability and CO_2 neutrality[1,4]. Biomass is defined as an organic material accumulated in plants via photosynthesis, and it can be obtained for example from wood, energy crops and agricultural residues[5]. Its versatility allows to obtain different products, like heat, power, transportation fuels, chemical compounds and biomaterials[6], but in order to do so it must go through a conversion process, which can be biological, mechanical or thermal. In this last category, we can find combustion, gasification and pyrolysis. Combustion is the simplest way to convert biomass in either heat or power and it is widely practiced commercially. However, it is not an environmentally-friendly option due to its low efficiency, high emissions and the generation of ash[6]. Gasification is one of the most efficient methods to convert biomass into fuels, but it requires high investment, transportation and storage costs[7]. On the other hand, pyrolysis has been accepted as a promising method as it balances reasonable costs with simple operation techniques.

Pyrolysis is a thermochemical decomposition process in which organic material is converted by heating in the absence of oxygen into a carbon-rich solid called biochar, a liquid fraction called bio-oil and gases[8]. Generally speaking, bio-oil has poorer physical and chemical characteristics compared to liquid fossil fuels. For example, a water content between 15-30%, which reduces the heating value of the oil, high acidity leading to corrosion, high viscosity and low chemical stability[9,10]. In order for these characteristics to improve and obtain a product of higher quality resembling diesel fuels, the bio-oil should go through an upgrading process.

Among the diverse upgrading techniques that have been suggested through the years, hydrodeoxygenation (HDO) appears to be the most auspicious route to produce biofuels through the upgrading of bio-oil due to a good economy of the input materials, the flexibility with respect to the biomass feed and its applicability in current infrastructure[11]. HDO is a high pressure process where hydrogen is used to remove O and saturate double bonds in the bio-oil. The most commonly used catalysts are sulfide, noble metal and transition metal catalysts[12]. Ni-based catalysts are becoming more and more attractive for industry, as they consume less hydrogen, their price is lower and they are widely available[13,14].

When possible, it is important to reuse the catalyst to its maximum extent in order to minimize the generation of waste materials. Therefore, the catalyst should be regenerated after each reaction[15]. Catalytic regeneration is a fundamental process that helps to increase its reusability and recyclability without having the catalytic activity compromised, and so extending its lifetime[16].

In this work, four different Ni-based catalysts were synthesized and tested for the HDO of beech wood bio-oil. Their characteristics were analyzed in different stages during their synthesis and

after the reaction. The resulting upgraded bio-oil products were also analyzed. According to these results, the catalyst with the best performance was selected, regenerated and used again in 3 subsequent reaction cycles. Finally, its stability and degree of deactivation were assessed.

2. Definition of tasks

Pyrolysis oil from lignocellulosic biomass is a complex mixture of organic compounds and solid particles. Its composition derives in some negative characteristics, such as an elevated O and water contents, low pH values, high viscosity and insolubility in other fossil fuels. To improve the quality of pyrolysis oil, an upgrading process called hydrodeoxygenation (HDO) can be used. HDO requires the utilization of a catalyst during the reaction. This is was the focus of this work.

The aim of this study was to synthesize and characterize four different Ni-based catalyst, while testing them for HDO of pyrolysis oil from beech wood biomass. First of all, the catalysts were prepared and analyzed using different methodologies in each step of their synthesis. Later on, they were employed in HDO reactions in determined temperature and pressure conditions. The resulting products were evaluated and compared considering particular criteria in order to determine the catalyst with the best performance. As a last step, the selected catalyst was regenerated and reused in three consecutive cycles (reactions) in order to test its recyclability and performance along its use.

3. Theoretical introduction

a. Pyrolysis oil from biomass

Biomass pyrolysis is defined as the thermal decomposition of biomass organic matrix in the absence of oxygen at very high temperatures. From this process, three main products are obtained: a solid phase called biochar, a liquid phase called bio-oil and non-condensable gas products[9,17]. During biomass pyrolysis, many different reactions occur at the same time, such as dehydration, depolymerization, isomerization, aromatization, decarboxylation and charring[9]. Some parameters that can influence this process are the type of biomass used, any physical, thermal, chemical or biological pretreatment and the reaction conditions (temperature, heating rate, reaction atmosphere)[1].

Bio-oil, which is also referred as pyrolysis oil, is a dark brown, viscous liquid containing a high amount of water (15-35%), hundreds of different organic compounds[18] and solid particles. Its HHV typically ranges between 15 and 20 MJ/kg, which represents only the 40-50% of conventional fossil fuels (42-45 MJ/kg)[19], mainly due to the high O content in the bio-oil. Apart from these, there are other undesirable characteristics that affect the quality of bio-oil. The presence of carboxylic acids leads to low pH values (2-3,7), that turn bio-oil into a potentially corrosive and highly unstable substance during storage due to continuous chemical reactions that form larger

molecules (polymerization, etherification and esterification)[20]. Moreover, it is non-miscible with other fossil fuels and, when it is stored for a long time, the viscosity increases and a separation of continuous and dispersed phases occurs. Considering these poor fuel properties, bio-oil could only be used in boilers and furnaces, being totally inappropriate for direct use in diesel engines or gas turbines[21].

In order to overcome these disadvantages and to turn bio-oil into a commercially accepted fuel that could potentially replace petroleum, a further upgrading is needed[22]. There are five ways to do this: catalytic cracking, HDO, steam reforming, esterification and through supercritical fluids[23]. HDO implies the removal of acidity through the esterification of free acids while eliminating water. Additionally, bio-oil can be used as feedstock for producing chemicals, such as phenols for resin production, additives in fertilizing and pharmaceutical industries and flavoring agents in the food industry[24].

b. Hydrodeoxygenation

HDO of bio-oil involves the presence of a catalyst and hydrogen at moderate temperatures (between 300 and 600°C). The O is removed in the form of water, which is environmentally benign[25]. Some of the reactions that take place during the HDO process are water separation, dehydration reactions due to the condensation polymerization reactions, decarboxylation reaction in which O is removed as water, HDO reactions which may involve the saturation of unsaturated components, hydrogenolysis reactions which are related to the cleavage of C-O bonds where the O may be released in the form of water, and hydrocracking reactions involving the breakdown of high molecular components into smaller molecules[11,26].

The amount of organic compounds containing O in them mostly depends on the origin of the feed. Generally speaking, one fourth of the liquids derived from lignocellulosic biomass is made up of phenols. Other types of O-compounds include ketones, aldehydes, carboxylic acids, esters, alcohols and ethers[25]. O contained in these molecules lead to undesirable properties such as low energy density, chemical instability, high viscosity and corrosion[10].

The presence of water in the bio-oil, generally ranging from 15% to 30%, is detrimental to the heating value and flame temperature of the fuel. Compared to other fossil fuels, these values are extremely high, while the S and N contents in bio-oil tend to be negligible. Therefore, HDO becomes an important research topic, which may boost bio-oil quality and achieve a fuel compatible with the petroleum fraction.

When assessing the price/availability relationship for biomass as feedstock, it is noticeable that the use of noble metal catalysts for HDO is an uneconomical alternative. Consequently, the research focus has been set to non-noble metals catalysts such as metals carbides, metal nitrides, metal borides and transition metal phosphides.[27]. Among them, Ni-based catalysts have generated growing interest due to their low prices and small hydrogen consumption.

c. Nickel-based catalysts and most common supports

Noble metal catalysts show high deoxygenation activity and yields. Some like Pt, Pd and Ru have been widely evaluated for the HDO process and are often the first choice in hydrogenation reactions. Additionally, they have a very low tendency to get poisoned by the amount of S present in the bio-oil[28]. However, their elevated prices prevent them from being widely used for industrial applications. That is why Ni-based catalysts are considered to be the most attractive alternative for the industrial application of the HDO process, mainly due to their low costs, non-sulfided nature and high activity[29]. As noble metal catalysts, Ni-based catalysts mainly give the decarbonylation/decarboxylation products but, unlike them, they generate more cracked products, which results in a lower diesel yield and an increased hydrogen consumption[30].

Bimetallic NiCu catalysts have also been widely tested. The addition of Cu could improve the dispersion of Ni and reduce its particle sizes[31]. The retention time of oxygenated hydrocarbons passing through the Ni is shortened, which weakens the dehydrogenation of Ni and slows down the conversion of oxygenated hydrocarbons to graphitic carbon[31]. A bimetallic catalyst consisting of Ni and Cu could activate hydrogen at a lower reaction temperature, which enhances hydrogenation and restrains polycondensation reactions at the same time. Ni easily dissociates hydrogen molecules, which then move to Cu sites, while the Ni sites are evacuated and able to absorb other hydrogen molecules. The lower dissociation barrier of Cu makes the hydrogen on Cu sites to be desorbed easily[31].

Two supports that are being more frequently used for HDO reactions are silicon dioxide (SiO_2) and zirconium dioxide (ZrO_2). SiO_2 is considered as an inert support of weak acidity, good selectivity and activity[32]. SiO_2-supported catalysts have a high specific surface area, a narrow range of pore size distribution and large pore volume[33], and have displayed a relatively low affinity for carbon formation[34]. On the other hand, ZrO_2 possesses an amphoteric character that helps preventing coke formation[35], interacts strongly with active species and influences the adsorption and redox properties of the catalysts[36]. However, it has a small surface area, which is detrimental to catalytic performance[37].

d. Catalyst characterization

i. Brunauer-Emmett-Teller (BET) method

Determining the surface area of a catalyst is of the utmost importance in order to understand how much the active metals can be dispersed. The higher the surface area of the support, the higher dispersion of the active metals, and therefore an increased catalyst activity is obtained[38].

The Brunauer-Emmett-Teller method (BET) is used to determine the surface area of porous materials such as catalysts and supports. The BET theory simplifies the adsorption of a gas over a surface and adopts the adsorption theory from Langmuir for the following conditions:

- Multilayer adsorption can occur on subsequent layers
- The adsorbing surfaces are homogeneous
- The heat of adsorption is independent of the degree of coverage
- No interdependence occurs between the adsorbed parts of a layer

This method is based on the adsorption and condensation of nitrogen at 77 K of temperature. First of all, the sample is evacuated at 403 K (130°C) and then cooled to 77 K by means of liquid nitrogen. The partial pressure of nitrogen on the sample is increased, which will lead to the adsorption of an amount of gas to the sample surface while being removed from the gas phase. Once it is stabilized, the pressure of the equilibrium and the quantity of adsorbed nitrogen at each pressure are recorded. With this data, an isotherm is plotted, describing the volume of adsorbed nitrogen in relation to the relative pressure p/p_0. The complete adsorption isotherm is reached when the pressure is increased until the saturation point. Afterwards, the pressure is slowly decreased and the desorption isotherm is recorded.

The BET equation creates a link between the volume of adsorbed nitrogen at a given partial pressure and the volume that is adsorbed when a monolayer covers the catalyst.

$$\frac{p}{v*(p_0-p)} = \frac{1}{v_m*c} + \frac{c-1}{v_m*c}*\frac{p}{p_0}$$

where p is partial pressure of nitrogen, p_0 is saturation pressure at the experimental temperature, v is volume of adsorbed nitrogen at pressure p, v_m is volume of adsorbed nitrogen at a monolayer and c is a constant.

From this equation, v_m is calculated and it is then used to determine the total number of adsorbed nitrogen molecules in the monolayer.

$$\text{Number of } N_2 \text{ molecules} = \frac{v_m(m^3)*6,02e^{23}(molecules/mol)}{0,0224(m^3/mol)}$$

As each adsorbed nitrogen molecule covers an area equivalent to its cross section ($0,162nm^2$), the total surface area of the catalyst can be calculated as the product of the number of nitrogen molecules and the surface occupied by each molecule.

$$SA(m^2) = No.N_2 molecules * 16,2e^{-20}(m^2/molecule)$$

ii. Temperature-programmed reduction (TPR)

The temperature-programmed reduction belongs to the thermo-analytical methods with which one can assess the characteristics and reactivity of heterogeneous catalyst systems[39]. It studies the

behavior of a material under reductive conditions, which are generally created by means of a hydrogen flow, either in a temperature range or at a given temperature.

The sample is first placed on a double-crib silica tube and dried in an argon flow at a temperature around 300°C. After being cooled down to 40°C, they are set in a furnace under a flow of reactive gaseous stream and heated up to a maximum of 900°C, depending on the sample under analysis. The gas flow is maintained constant along the measurement and the temperature is linearly increased at a certain heating rate. During the reduction, the gas composition, and therefore the hydrogen content, is quantified at the outlet of the reactor. A thermal conductivity detector (TCD) is used to measure changes in the thermal conductivity of the gas stream. The TCD signal is converted to concentration of active gas using a level calibration. As a result, the relation between temperature and hydrogen consumption is plotted. The area under the peak represents the total amount of consumed hydrogen in moles of hydrogen per mole of metal atom, and is later used to calculate the degree of reduction and average oxidation state of the solid material[38].

The parameters that affect the TPR profiles are the heating rate (in K/s), the initial amount of reducible species (in µmol), the flow rate of the reducing gas mixture (cm^3/s) and the concentration of hydrogen in the carrier gas (in $\mu mol/cm^3$). For instance, when the heating rate increases, the reduction peak will appear later at a comparatively higher temperature than at a lower heating rate. Additionally, if there is an increase in the concentration of hydrogen in the reductive gas flow, the samples will be reduced more easily, resulting in sharper peaks at lower temperatures. While the gas flow rate has little effect, a higher initial amount of the samples will lead to a greater area under the reduction peak.

TPR, together with temperature-programmed desorption (TPD), forms a class of techniques in which a chemical reaction is monitored while the temperature increases linearly in time. These techniques are applicable to real catalysts and single crystals. The basic setup consists of a reactor and a thermal conductivity detector to measure the hydrogen content of the gas mixture before and after the reaction. More sophisticated TP equipment contains a mass spectrometer for the detection of reaction products.

iii. Scanning electron microscopy - Energy dispersive X-ray analysis (SEM-EDX)

This method assists in detecting the presence of different inorganic and organic elements on the surface of the catalyst[40]. The interaction between the electron beam and the sample generates an X-ray that is used for its chemical analysis: when high energy, secondary and backscattered electrons interact with the surface of the sample, characteristic X-rays are emitted, which means that their wave lengths are distinctive of the atoms present in the sample.

These X-rays enables to characterize any kind of solid material. The energy and wavelength of X-rays are different for each atomic species and by measuring them, the elements present in the

sample can be detected and quantified. From the X-ray spectra, both qualitative and quantitative analyses can be done. If one measures the wavelength and the energy of each characteristic emitted X-ray, the elements present in the sample can be identified. This corresponds to a qualitative analysis. On the other hand, if one measures the emitted X-rays per time unit, the amount of the element present in the sample can be determined. This is a quantitative analysis[38].

The equipment used for this test is composed of an energy dispersive spectrometer or an EDX detection system, which can detect most of the X-ray spectrum. Typically, the detector consists of semiconducting silicon or germanium and is placed very near in line with the sample (approximately 20 mm).

iv. X-Ray Diffraction (XRD)

The main aim of X-ray diffraction (XRD) is to determine the crystal structure of a material. It is based on the ability of energetic X-rays wave lengths to penetrate solids, which allows to identify bulk phases and estimate particle sizes. Generally, crystalline materials having crystal domains greater than 3-5 nm are detected. These types of materials consist on atoms arranged in a regular, organized three dimensional pattern, called crystal structure. Polycrystalline materials are formed by many small crystal regions known as grains, which are separated by boundaries. These grains can have different shapes and sizes and are disorientated with respect to each other[38].

This technique requires samples with sufficiently long range order. Consequently, amorphous and small particles produce broad and weak diffraction lines, or even none at all[41].

The catalyst samples, which are prepared as a fine powder, are impacted with X-ray beams. The crystal structure of the sample diffracts the beams, allowing one to derive lattice spacing by measuring the angles (2θ) under which constructively interfering X-rays with wave length λ leave the crystal. For this, the Bragg's law is used.

$$n * \lambda = 2 * d_{hkl} * \sin \theta_{hkl}$$

where n is an integer, λ is the x-ray wave length, d_{hkl} is the perpendicular spacing between two lattice planes hkl and θ_{hkl} is one half of the diffraction angle.

The angle and intensity of the reflected beam are measured with a diffractometer and, as a result, a diffractogram is obtained, in which the distribution of intensity along the angle area is drawn. With the help of a data bank, one can identify the underlying substance and identify its crystal structure. Additionally, the crystallite size can be calculated through the Scherrer equation[42], after identifying the position of the peak and its FWMH (full width at half maximum) value.

v. Inductively coupled plasma - Optical emission spectroscopy (ICP-OES)

In order to determine the metal composition of the catalysts as well as the concentration of S and the metal content of the bio-oil samples[43], the ICP-OES (inductively coupled plasma - optical emission spectroscopy) is used. In this technique, the composition of elements in water-dissolved samples can be determined by means of a spectrometer and plasma.

The sample should first be dissolved in water and, with the help of a peristaltic pump, go through a nebulizer into a spray chamber to produce an aerosol. This aerosol is then led into an argon plasma, which is generated at the end of a quartz torch by a cooled induction coil with a flow of high-frequency alternate current. Consequently, an alternate magnetic field is induced, which accelerates electrons into a circular trajectory and leads to the ionization and later stabilization of the plasma.

The temperature of the argon plasma can range between 5000 and 10000 K. The electrons gain this thermal energy and reach a higher energy state. As the electrons lose this energy and return to their original level, photons are liberated. Every element has its own emission spectrum: a spectrometer measures the light intensity on the wave length and after a calibration, this result is converted into a concentration of the desired element[44].

e. Bio-oil characterization

i. Elemental analysis and physicochemical properties

Evaluating the elemental composition of the bio-oil is of the utmost importance, as it is the only technique that allows to determine how much O is removed during the HDO process. Moreover, the determination of the carbon content in the upgraded bio-oil enables to predict its quality: more elemental carbon means more carbon available to burn and convert to CO_2[45].

The physicochemical properties considered in this study are pH, density and higher heating value (HHV). Apart from removing O from the bio-oil, other aims of the HDO reaction is to increase its pH value, decreases its density and increase its HHV, so that the resulting upgraded bio-oil improves its quality and resembles diesel fuels. Higher pH values reduce the corrosive behavior of the fuel, lower densities promote an easier fluidity and injection in the diesel engine and higher HHVs indicate that more energy will be delivered per mass unit of fuel.

ii. ^{1}H- Nuclear Magnetic Resonance (^{1}H-NMR)

This method is used to determine the content of carbon and hydrogen and the structure of the molecules of samples. NMR spectroscopy uses a large magnet to investigate the intrinsic properties of atomic nuclei. As for every spectroscopy, NMR uses a component of electromagnetic radiation to produce resonance, that is, transitions between nuclear energy levels.

NMR spectroscopy is related to the movement of the nuclear spin. Atomic nuclei with an uneven number of protons or neutrons dispose over a magnetic momentum and are therefore NMR-active. Atomic nuclei that have such behavior are for example ^{1}H, ^{13}C, ^{15}N, ^{19}F and ^{31}P. However, ^{12}C and ^{16}O are NMR-inactive, as they have an even number of neutrons and therefore cannot build a magnetic momentum[39].

All molecules with a non-zero spin have a magnetic moment. The magnetic moment of the nucleus forces it to behave as a small bar magnet. In the absence of an external magnetic field, each magnet is randomly oriented. But during the NMR experiment, the sample is placed in an external magnetic field which forces the bar magnets to align with (low energy) or against (high energy) the external magnetic field. During the measurement, a spin flip of the magnets occurs, requiring an exact quanta of energy. In order for the NMR experiment to work, a spin flip between the energy levels must take place[46]. This flipping process is based on the ability of atomic nuclei to align at will and adjust their direction relatively to a static, homogeneous magnetic field. The atomic spin is taken through the outer magnetic field from a low energy state α to a higher energetic state β. The necessary energy supply needed to overcome the difference between the two spin states is in the radio waves region[39].

As a result of the measurement with the spectrometer, a FT-NMR spectrum is obtained. The chemical shift δ is the relation between the distance from the reference signal and the operating frequency of the spectrometer, and it is expressed in ppm (parts per million).

$$\delta(ppm) = \frac{\text{distance from reference signal (Hz)}}{\text{operating frequency of the spectrometer (MHz)}}$$

The radiation energy, and so the chemical shift, that is required by a proton to flip, depends on the nuclei locations, the intensity of the magnetic field and the chemical surroundings of the nuclei.

iii. Gas chromatography - Flame ionization detector (GC-FID)

The combination of a gas chromatographer with a flame ionization detector (FID) assists in quantitatively determining the organic bonds. For this study, this technique was used to analyze the gas sample obtained from the reactor after the HDO. In the GC, the carrier gas current with the analyzed components is directed to the flame. The principle is based on the conductivity of the free electrons produced during the ionization in the flame. The flame tops works as cathode, while the collecting electrode works as anode. The intensity of the current is measured and a spectrogram is obtained, which shows the individual peaks for each bond according to the retention time. The characteristic retention time allows to recognize the different types of bonds in a mixture of materials. A qualitative analysis, for example GC-MS, is then necessary to organize the peaks and their surfaces of each substance.

The surface of the peaks allows to calculate the concentration of each component in the sample. Additionally, a standard component in a fixed concentration in the sample is necessary, in order to

correlate the peak surfaces in the spectrogram to it. According to the desired precision, each material must be calibrated and correction factors must be calculated[39].

f. Catalyst regeneration

One of the problems that occur more often to HDO catalysts is deactivation, that is, the loss of activity by the catalyst. This can be produced by coke deposition, sintering, poisoning or metal deposition[10]. Among them, coke deposition is particularly frequent and harmful, mainly due to polymerization and polycondensation reactions. The sharp difference in the average molecular weight makes the adsorbed reactants have a significant effect on the degree of deactivation of the catalyst[10].

The stability of many HDO catalysts, and in particular Ni-based catalysts during HDO of pyrolysis oil, has not been studied much[40]. In fact, most works only consider one regeneration step and do not contemplate Ni catalysts[40,47,48]. In this study, more regeneration steps were done and four different Ni-based catalysts were tested. The stability of a selected catalyst was monitored in a number of consecutive cycles using the methods mentioned above.

4. Objectives

The main aim of this work is to test the performance of four different Ni-based catalysts in the upgrading of beech wood bio-oil and, based on the analysis of the resulting products, select the catalyst with the best performance. This catalyst will be later regenerated and reused in 3 consecutive reaction cycles and a suitable, cost-effective course of action for HDO of bio-oil will be proposed.

5. Methodology

a. Catalyst and support selection

The reason for choosing Ni-based catalysts (in this case, Ni/SiO_2, Ni/ZrO_2, $NiCu/SiO_2$ and $NiCu/ZrO_2$) is their high abundance, low price, reduced hydrogen consumption and a smaller tendency to poisoning compared to noble metal catalysts[14,49]. Besides, it has been proven that the addition of Cu simplifies the reduction of Ni oxide at lower temperatures[50] and decreases the coke formation rate[51]. SiO_2 was selected as support because of its inert character, weak acidity and good selectivity and activity[32]. On the other hand, ZrO_2 was also used as support due to its small tendency to coke formation and high catalytic activity[37].

b. Catalyst synthesis

Four Ni-based catalysts were prepared by the wet impregnation method with aqueous solutions of the precursors: Ni/SiO_2, Ni/ZrO_2, $NiCu/SiO_2$ and $NiCu/ZrO_2$. The metal precursors were $Ni(NO_3)_2{\cdot}6H_2O$ (Sigma-Aldrich) and $Cu(NO_3)_2{\cdot}2H_2O$ (Alfa Aesar). For the monometallic Ni catalysts, the metal concentration was 8.6 wt%[34], while for the bimetallic catalysts, the metal concentration was 28 wt% Ni and 3.5 wt% Cu[52]. The metal precursors were dissolved in distilled water. Both supports (Alfa Aesar), which were in the shape of pellets, were milled to a fine powder by means of a Waddel disk with a fraction of 0.125-0.250 mm (diameter inferior to 100 µm) and later added to the previous solution with a ratio weight support/solution circa 1:10. The water in the solution was evaporated using a rotary evaporator (Hei-VAP Advantage ML/G3) and the formed catalyst was dried overnight in an oven at 105°C. Afterwards, all catalysts were calcined in air at 450°C for 4 hours after reaching the set point, with a heating ramp of 10°C/min (Thermolyne F6010), and later reduced in a 25% H_2/N_2 flow of 3 l/min, with a heating ramp of 5 K/min for 4 hours, using reduction temperatures below 500°C (according to TPR results, see Section 6.a.i).

c. Reactions setup for HDO reactions

i. Reactor

For all the experiments carried out in this study, a 200 ml autoclave made of Inconel alloy 625 was used. It was built at IKFT/KIT and designed for a maximum pressure of 360 bars and a maximum temperature of 400°C. It was equipped with a magnetically coupled stirrer (torque 80 N·cm, Premex reactor AG) and a gas injection stirrer, which simplifies the mass transfer of hydrogen in the liquid medium. The heating system consisted of heating cartridges inserted in a brass mantle, whose power input was controlled by a self-made Labview programme.

ii. Reaction conditions

The reactor was filled with 50 g of beech wood bio-oil supplied by Biomass Technology Group (BTG Enschede, The Netherlands), from which 20,5 g were heavy phase and 29,5 g light phase, and 2,5 g of the corresponding reduced Ni-catalyst. Before loading the reactor with hydrogen (Air liquid

Alphagaz 2, purity 6.0), it was purged with nitrogen for 5 minutes. A fine catalyst powder and the maximum speed rate of the stirrer (1000 rpm) were used as a way to enhance mass transfer and promote HDO over polymerization reactions.

Once the reagents were inserted in the autoclave, the reactor was closed and pressurized with hydrogen up to 80 bars at room temperature. The stirrer was switched to 1000 rpm and the heating program was started until it reached 325°C. The global reaction time, including the heating ramp, was 120 minutes. When this time was reached, the reaction was quenched first using a flow of compressed air, and later in an ice/water bath until the internal temperature reached 17°C. Each experiment was performed twice and the results are reported as an average.

iii. Recovery of the products

After the reactor had been cooled down, a gas sample was taken and analyzed by gas chromatography. The liquid and solid products were collected from the reactor and centrifuged at 7000 rpm for 40 minutes (Thermo Scientific Heräus Biofuge Stratos, fixed angle rotor 26 n.75003014). The products were separated in an aqueous phase, a heavy phase or upgraded oil and a solid phase consisting of the catalyst and carbon deposition. The aqueous and heavy phases were separated and weighted. The residues in the reactor, mainly comprising catalyst, solid and tar-like components, were collected by washing the reactor walls with acetone. This fraction, together with the solid fraction resulting from the centrifugation step, was washed with acetone and filtered with a Whatman filter (Grade 589/3 blue ribbon), in order to recover the catalyst that would be used in further regeneration reactions. The carbon content of the solids formed during the reaction was determined by elemental analysis of the spent catalyst.

iv. Calculation of the hydrogen consumption and gas production

First of all, from the ideal gas equation (1), the number of moles of hydrogen added to the reactor was calculated. From the results obtained from the GC-FID measurement of the gas sample and the final hydrogen pressure in the reactor, the total number of moles was determined. Using the equation 2, the partial pressure of hydrogen was obtained. Afterwards, with the equation 3, one can calculate the number of moles of hydrogen and then, through equation 4, determine the proportion of hydrogen that was consumed during the reaction. Subsequently, the number of moles of hydrogen consumed by mass unit of bio-oil is calculated, and later transformed into normal liter (NL) of hydrogen per kilogram of bio-oil.

$$P*V = n*R*T \quad (1)$$

$$P(H_2) = x(H_2)*P_{Tot} \quad (2)$$

$$P(H_2)*V = n(H_2)*R*T \quad (3)$$

$$P(H_2)*V=n(\%\,H_2 consumed)*\left[100-\frac{n(H_2\,final)}{n(H_2 initial*100)}\right] \quad (4)$$

For the estimation of each gas produced, the global amount of moles contained at the end of the reaction was multiplied for the component fraction measured by GC.

v. Calculation of the mass balance

To calculate the mass balance, the values of the total recovered products (aqueous phase, oily phase, catalyst and solids), the separated aqueous phase, the mass of catalyst in the reactor and the mass of produced gas were registered. Afterwards, the mass of the solids was calculated taking into account the percentage of carbon present in the spent catalyst (considering that the solid residue is mainly composed of carbon depositions) and the mass of catalyst in the reactor (equation 5).

$$m_{solid}=\frac{\%C_{sp.catalyst}*m_{catalyst}}{100-\%C_{sp.catalyst}} \quad (5)$$

The phase corresponding to the upgraded oil was obtained as the balance between the masses of the recovery (which is the sum of the masses of the aqueous phase, the heavy phase, the catalyst and the solids), the aqueous phase, the catalyst and the solids. The total mass of products was calculated as the addition of the oily phase, the aqueous phase, the solids and the gas production. Moreover, the mass of the feed was registered as the sum of the heavy phase and the light phase that had been introduced in the reactor before the reaction. The difference between the total feed and the total mass of products results in the losses.

d. Catalyst characterization

The catalyst metal content was determined by ICP-OES using an Agilent 725 ICP-OES Spectrometer, after pre-digestion of the sample with HNO_3, HCl and H_2O_2 in a microwave oven (600 W, max 6 MPa, 240°C, 45 min).

To determine the reduction temperature profile of the active metal, the temperature programmed reduction (TPR) was measured with an Autochem HP 2950 (Micrometrics) using a heating rate of 1 K/min until reaching 500°C and 5% H_2 in Ar with a global flow of 30 ml/min. The samples had been dried in a 30 ml/min flow of Ar at 300°C for 3 hours before the measurement.

The total specific surface area of the catalyst was determined by nitrogen physisorption with a Belsorp Mini II at 77K and calculated by applying the BET theory in the fitting rate between 0.05-0.30 p/p_0 (12 points).

Powder X-Ray diffraction (XRD) was measured using an X'Pert PRO MPD instrument (PANalytical GmbH) equipped with a Cu anode (Cu Kα 1.54060 Å). The XRD patterns were recorded in a 2θ range between 5° and 120° (1 hour, step size 0.017°). The average crystallite size was estimated using the Scherrer equation (shape factor used K=0.9) after correcting the instrumental line broadening.

Leaching of the catalyst was monitored by analyzing the aqueous phase by ICP-OES (Agilent Technologies 700 Series, 5100 SUDV). Sample preparation implied the filtration with a 0.2 µm PTFE membrane of the produced aqueous phase after each reaction.

In order to identify the elements present on the catalyst surface in the fresh and spent forms, SEM-EDX (Scanning Electron Microscopy-Energy Dispersive X-ray spectroscopy) was used. The equipment for this technique was GeminiSEM 500, Zeiss, software SmartSEM Version 6.01, with a thermal Schottky field emitter cathode. An energy dispersive X-ray spectrometer X-MaxN from Oxford with a silicon drift detector (80 mm^2 and resolution of 127 eV) was employed for the quantitative analysis of micro areas and the distribution of the elements, in addition to the software Aztec 3.3.

Carbon deposition, S and N content were assessed by elemental analysis. C, H, N and S of the spent catalysts were measured on a micro-elemental analyzer Elementar Vario el Cube.

e. Characterization of the upgraded products

The pH values were measured with a laboratory pH-meter Metrohm. The HHV was determined using a calorimeter IKA C5000 control. For the water content in both upgraded oil and aqueous phases, a volumetric Karl-Fischer titrator from Metrohm (Titrando 841) was used, with the titration reagents Composite 5 and Methanol dry. Carbon, hydrogen and N content were measured using a micro-elemental analyzer Elementar Vario el Cube. Elemental composition and the physicochemical properties of the upgraded oil were contrasted with the properties of the original beech wood bio-oil used as feed (Table 1)[53].

Table 1: Physicochemical properties and elemental analysis (in wet basis) of the heavy phase (HP) and light phase (LP) of BTG beech wood bio-oil before hydrotreatment over Ni-based catalysts.

	Beech wood bio-oil	
Phases	**HP**	**LP**
Composition (%)	59	41
C (wt.%)	54,3	34,3
H (wt.%)	7,5	8,3
N (wt.%)	0,2	0,2
O (wt.%)	38,2	57,3
H_2O (wt.%)	14,5	35,3
HHV (MJ/kg)	23,1	14,1
pH	3	2,7
Density (g/cm^3)	1,19	1,17

Quantitative ^{1}H-NMR was employed to calculate the concentration of protons associated to the chemical shift range, typical of some functional groups. NMR spectra were recorded at 25°C on a Bruker Biospin spectrometer, equipped with a 5.47 T magnet (^{1}H frequency 250 Hz). Sample preparation consisted of 0.1 g of either upgraded bio-oil or aqueous phase and their dilution in 0.7 g of deuterated methanol (MeOD) containing TMSP-d4 (3-(trimethylsilyl)-2,2,3,3-tetradeuteropropionic acid) as internal standard (0.1 g TMSP in 50 ml MeOD). Subsequently, the samples were centrifuged in order to remove eventual undissolved particles in the solution and placed in NMR tubes.

f. Catalyst regeneration

The performance of each catalyst was assessed by contrasting the elemental composition and water content of the upgraded oil, paying special attention to carbon and O content, and their hydrogen consumption. The catalyst with the best performance was selected and regenerated in order to observe structural and chemical variations and changes in activity in comparison to the original catalyst.

Two more original HDO reactions were carried out with that catalyst in order to acquire more solid material for the further regeneration steps. Afterwards, the spent catalysts from the four original reactions were mixed and calcined in air at 450°C for 4 hours in order to eliminate the carbon and later reduced in the same conditions as the fresh catalyst. Experiments with the regenerated catalyst were performed again using the same conditions described for the fresh catalyst. In this work, three regeneration steps were done. The spent catalyst was analyzed through SEM-EDX and XRD in between regenerations: EDX was performed for the spent and reduced catalysts, whereas XRD was performed for the spent, calcined and reduced catalysts.

6. Results and discussion

a. Catalyst characterization

i. TPR

The results obtained from the TPR were useful to identify the temperatures at which each catalyst should be reduced before being employed in the HDO reactions. For each one of them, the relation between the temperature and the TCD signal was plotted.

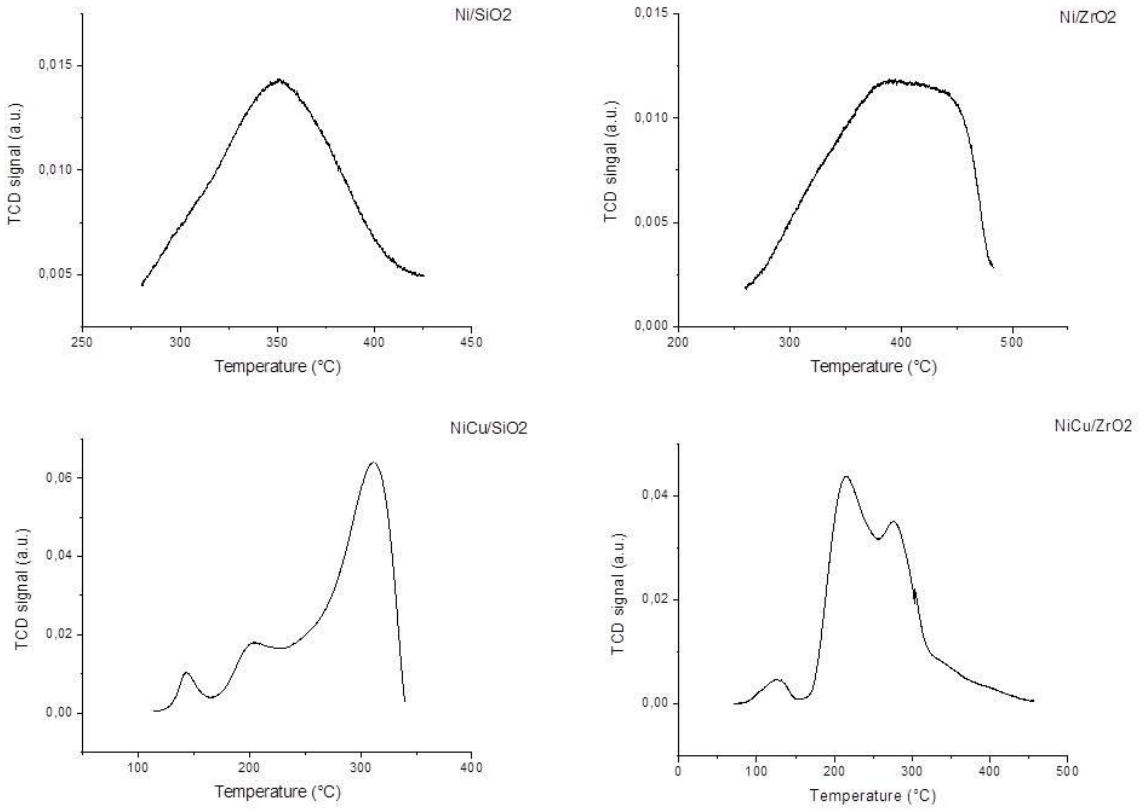

Figure 1: Temperature programmed reduction (TPR) of the catalysts of the four catalysts prepared for this study.

The TPR profile for Ni/SiO_2 shows a clear peak at 350°C, while the peak for Ni/ZrO_2 is found between 350°C and 400°C. Both profiles are in close relation with the ones obtained by other authors[43,54,55]. As the reduction of bulk Ni oxide occurs around 400-450°C[56,57], it was decided to set the reduction temperature of Ni/SiO_2 and Ni/ZrO_2 at 500°C in order to ensure a full reduction before its utilization in the HDO reactions.

It is known that the addition of Cu to Ni catalysts promotes the reduction of Ni oxide[56,57]. As it could be observed in our measurements, the peak temperature for both bimetallic NiCu catalysts is lower than for the monometallic Ni catalysts. In the case of $NiCu/SiO_2$, this value was clearly

located at 300°C, while for $NiCu/ZrO_2$ it was closer to 200°C, as it has also been found by Ardiyanti et al. and Jones[39,58].

Different peaks are present in the TPR profiles. As it was mentioned above, the reduction of bulk Ni oxide occurs around 400°C and 450°C. The reduction of Cu(II) to Cu(0) occurs in the region around 250°C, whereas the peaks located after these values (between 290°C and 390°C) are associated to the reduction of bimetallic NiCu species. Consequently, the selection of the reduction temperature for NiCu catalyst was made considering this information: a temperature of 350°C was chosen.

ii. SEM-EDX

EDX assists in detecting the presence of elements with atomic numbers Z greater than 4 on the surface of the catalysts. In this study, the fresh catalyst (that is, before the HDO reaction) and the spent one (after the first HDO reaction) were contrasted for the four Ni-based catalysts tested (Table 2).

In the case of Ni/SiO_2, it can be observed that some carbon is deposited on the catalyst surface once it is used in the reaction: the carbon concentration increases from 3.6 wt.% to 13.8 wt.%. Moreover, a small amount of sulfur near the detection limit appears on the surface in the spent form, giving signs of low poisoning of the catalyst. As a result of these two effects, it can be seen how the proportion of Ni on the catalyst surface decreases, indicating that is being covered mainly by the carbon deposits probably produced by the deposition of some higher molecular weight polymerization products[55].

Ni/ZrO_2 shows a very similar behavior. Very elevated carbon deposition with a difference of 20 wt.% between the fresh and the spent forms was observed, in addition to some poisoning by sulfur, calcium and iron, though in very small amounts. This led to a reduction in the concentration of Ni on the catalyst surface after the reaction.

On the other hand, $NiCu/SiO_2$ did not display high levels of carbon deposits like Ni/SiO_2 or Ni/ZrO_2, and so the concentration of Ni and Cu on the surface were not significantly affected during the HDO. There was however some sulfur poisoning, as in the two previously evaluated catalysts.

Finally, $NiCu/ZrO_2$ showed, like Ni/ZrO_2, the highest carbon deposition levels, with a difference of 20 wt.% between the fresh and the spent form. This affected strongly the concentration of Ni and Cu on the surface, reducing the first one in 21.2% and the second one in 28.3%. Additionally, some sulfur, calcium and iron poisoning appeared after the reaction.

Table 2: Concentration of elements present on the surface of different Ni-based catalysts before and after HDO (325°C, 80 bar hydrogen at room temperature).

Catalyst	Form	Ni (wt%)	Cu (wt%)	Si (wt%)	Zr (wt%)	O (wt%)	C (wt%)	S (wt%)	Ca (wt%)	Fe (wt%)
Ni/SiO_2	Fresh	11.2	-	38.6	-	46.6	3.6	-	-	-
	Spent	6.5	-	36.7	-	42.9	13.8	0.1	-	-
Ni/ZrO_2	Fresh	8.6	-	-	60.9	18.9	6.4	-	-	-
	Spent	6.3	0.7	-	45.5	18.8	26.3	0.1	0.1	1.3
$NiCu/SiO_2$	Fresh	30.0	2.9	29.2	-	34.7	3.2	-	-	-
	Spent	29.3	3.1	27.5	-	32.1	7.7	0.2	-	-
NiCu/ZrO $_2$	Fresh	55.8	6.3	-	20.0	13.6	4.0	-	-	-
	Spent	44.0	4.5	-	16.4	7.7	24.3	0.1	0.1	0.7

iii. XRD

XRD gave information about the crystalline structure of the catalyst. Figure 1 shows the structure of Ni/SiO_2 and Figure 3 shows the structure of $NiCu/SiO_2$. Both SiO_2-supported catalysts presented the same XRD patterns. In the calcined form, several peaks were detected. The first peak was located at 21.98°, clearly corresponding to the support (used as reference in Figure 1). The peaks located at 37.25° and 43.29° indicate the presence of Ni oxide (NiO). Additionally, metallic Ni was identified due to the peaks at 44.49°, 51.85°, 76.38°, 92.93° and 98.44°. Once the catalyst is reduced, the peaks for NiO disappear, leaving just the peaks for metallic Ni and the support left. The spent form of Ni/SiO_2 did not show any variations from the reduced form, which accounts for the stability of the catalyst.

A similar behavior can be seen for Ni/ZrO_2 in Figure 2 and $NiCu/ZrO_2$ in Figure 4. The first diffraction pattern from the bottom shows the reflections of the support ZrO_2, with reflections located at 27.95°, 31.362°, 34.06°, 49.21° and 50.37°. In the calcined form, both NiO and metallic Ni are present, although the reflection for NiO vanishes once the catalyst is reduced. Like the SiO_2-supported catalysts, the spent Ni/ZrO_2 and $NiCu/ZrO_2$ did not vary from the reduced form.

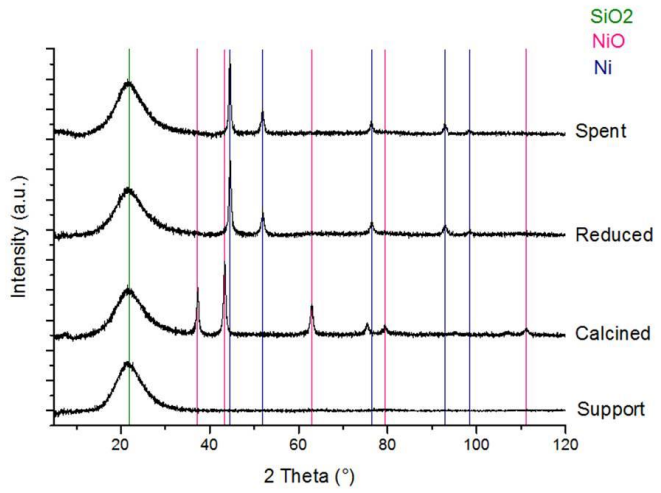

Figure 2: Diffractogram from the support SiO_2 and Ni/SiO_2 in the calcined, reduced and spent forms.

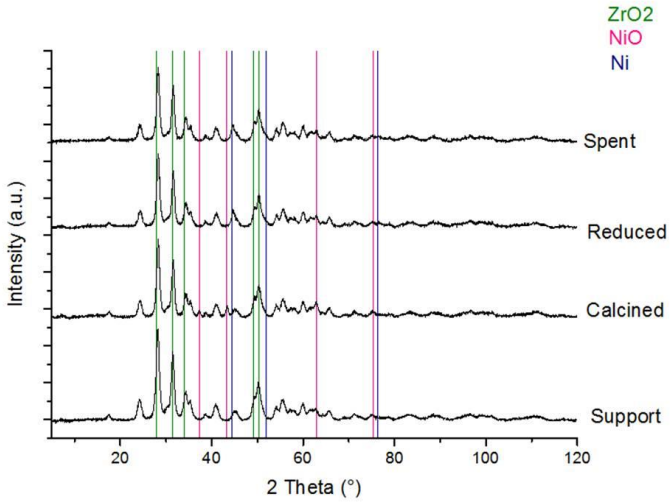

Figure 3: Diffractogram from the support ZrO_2 and Ni/ZrO_2 in the calcined, reduced and spent forms.

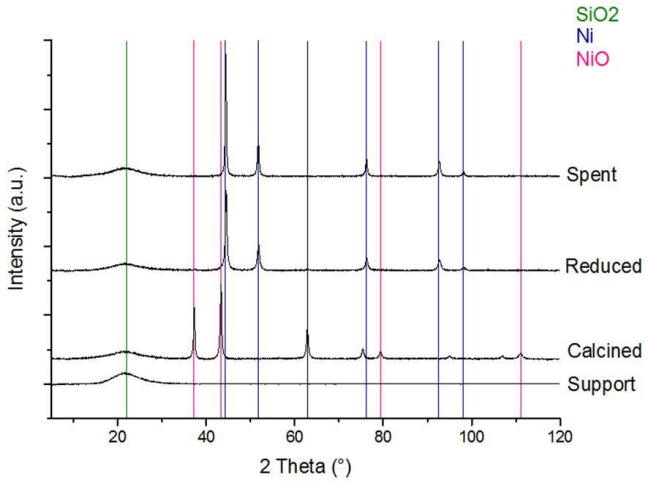

Figure 4: Diffractogram from the support SiO_2 and $NiCu/SiO_2$ in the calcined, reduced and spent forms.

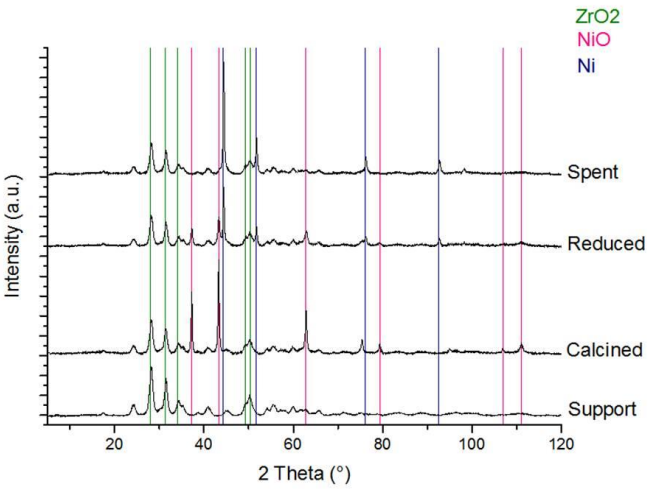

Figure 5: Diffractogram from the support ZrO_2 and $NiCu/ZrO_2$ in the calcined, reduced and spent forms.

The crystallite sizes were calculated using the results obtained with the XRD patterns and the Scherrer equation. For Ni/SiO_2, the crystallite size was 17.7 nm in the reduced form. This value increased to 20.85 nm after the catalyst was used in the reaction. In the case of $NiCu/SiO_2$, the values started at 21.4 nm after reduction and later increased to 42.95 nm after being used in the reaction. Haasterecht et al. [59] and Yin et al. [60] observed an increase in the cystallite size from the reduced to the spent form, the first in Ni/CNF (nickel supported on carbon nanofibers) catalysts tested in the aqueous phase reforming of ethylene glycol and the second in the catalytic hydrotreatment of fast pyrolysis liquids over NiCu catalysts. On the other hand, Ni/ZrO_2 displayed a 9.7 nm crystallite size after reduction, which decreased to 7.6 nm in the spent form. In a similar

way, NiCu/ZrO_2 showed in the reduced form a crystallite size of 43.3 nm, which was reduced to 41.45 nm in the spent form. Such a tendency has been also found in the HDO of 4-methylphenol over unsupported MoS_2, MoO_2 and MoO_3[61]. The reduction of the crystallite size was found only for the ZrO_2-supported catalysts. An explanation for this behavior could be given by Stichert and Schüth[62], who found that a more diluted concentration of the stock solution while synthesizing ZrO_2 would lead to the precipitation of smaller precursor primary particles, which reduces their crystallite size after being exposed to very high temperatures.

iv. BET method

As it was mentioned previously, the BET method assists in determining the surface area of the catalyst and, consequently, the potential dispersion of the active metals. Table 3 shows the results obtained for the four Ni-based catalysts in their fresh and spent forms[38].

Table 3: BET surface area of the catalysts used in this study in the fresh, spent and regenerated form.

	Ni/SiO_2		**Ni/ZrO_2**		**NiCu/SiO_2**		**NiCu/ZrO_2**	
	Fresh	Spent	Fresh	Spent	Fresh	Spent	Fresh	Spent
BET surface (m^2/g)	214.72	46.14	65.40	56.90	156.07	35.65	50.27	36.06

Ni/SiO_2 displayed the highest surface area in the fresh form (214.72 m^2/g), while NiCu/ZrO_2 had the lowest (50.27 m^2/g). As it was stated by Wang et al.[63], SiO_2-supported catalysts generally display a higher surface area than the ZrO_2-supported catalysts. Furthermore, the elevated value for Ni/SiO_2 could indicate a larger catalyst activity compared to the rest of them, due to the fact that a high surface area, in addition to a well-developed pore structure, is beneficial to an elevated dispersion of the active components and so an improved catalytic performance[64]. Boscagli et al. observed a BET surface area of 170 m^2/g for Ni/SiO_2 (metal loading of Ni 22 wt.%) and 110 m^2/g for Ni/ZrO_2 (metal loading of Ni 5.8 wt.%)[43]. These differences with the results obtained in our study could be based on the change in metal concentration in the catalysts, which for the monometallic Ni catalysts was 8.6 wt.%. The preparation method may also affect the surface area and therefore the dispersion of the active components, but in both cases wet impregnation was used[64].

It is clearly noticeable how the BET surface area dropped after the catalyst was used for the HDO reaction. All four cases showed this tendency, although it was smaller in the ZrO_2-supported catalysts, probably because of their initially low surface area. Many authors have documented this behavior and explained that one of the main reasons is the carbon deposition on the catalyst surface[63–66]. This can be easily confirmed when contrasting with the EDX results (see above), paying special attention to the Ni and carbon concentrations: the rise in carbon indicates char deposition on the catalyst surface, a reduction in its BET area and blockage of the active sites, leading to a lower amount of metal on the surface.

v. ICP-OES

This technique allows to contrast the metal composition of the catalysts before and after the HDO reactions. For Ni/SiO_2, a significant increase in the concentration of sulfur and potassium can be observed, while in the case of Ni/ZrO_2, the concentrations of calcium, sulfur and magnesium rise considerably (Table 4). Even if these metal concentrations are quite low in general, they are a visible sign of catalyst poisoning. For these two catalysts, it can also be observed how the concentration of Ni decreases from the fresh to the spent form. This indicates a loss of the active metal that is probably leached to the aqueous phase of the upgraded oil, which can be later confirmed when performing the ICP-OES of the resulting aqueous phases.

In the case of NiCu catalysts, a rise in sulfur concentration could be observed for both catalysts. For $NiCu/SiO_2$, also the concentration of potassium increased after the HDO reaction, while for $NiCu/ZrO_2$, an increase in calcium concentration could be observed. For both catalysts, the concentrations of Ni and Cu, the two active metals, decrease after the HDO reaction. As it could be observed in Table 2, considerable levels of carbon deposition were found on the catalysts surfaces. This may be the main reason why the metal concentration is reduced, followed by the possibility of leaching to the aqueous phase of the upgraded oil, as it was previously stated for Ni catalysts.

Table 4: Metal content of the different Ni-based catalysts in their fresh and spent forms after the HDO reactions (325°C, 80 bar hydrogen at room temperature).

Catalyst	Form	Ca (wt.%)	S (wt.%)	K (wt.%)	Mg (wt.%)	Ni (wt.%)	Cu (wt.%)
Ni/SiO_2	Fresh	0.036	0.010	0.005	0.010	7.940	0.001
	Spent	0.034	0.118	0.025	0.015	7.055	0.014
Ni/ZrO_2	Fresh	0.015	0.010	0.016	0.001	8.020	0.001
	Spent	0.064	0.131	0.004	0.015	6.940	0.073
$NiCu/SiO_2$	Fresh	0.026	0.010	0.004	0.007	27.900	3.250
	Spent	0.019	0.128	0.016	0.006	25.900	2.760
$NiCu/ZrO_2$	Fresh	0.014	0.010	0.003	0.002	27.300	3.100
	Spent	0.047	0.137	0.005	0.010	25.250	2.720

b. Characterization of upgraded products

i. Physicochemical properties, elemental composition and mass balance

The physicochemical properties analyzed for the upgraded bio-oil were the water content, higher heating value (HHV), pH and density (Table 6). For the water content, it was observed that after the HDO reactions, the amount of water in the oil was drastically reduced: from 14.5 wt.% in the HP in the original feed to values between 4.85 and 7.30 wt.% in the upgraded oils. In fact, more than half of the water content in the original oil was removed after the hydrotreatment. When

comparing among catalysts, the upgraded oil over Ni/SiO_2 showed the lowest water content (4.85 wt.%), while $NiCu/SiO_2$ had the highest value (7.30 wt.%).

The HHV was also considerably modified after the reactions. In the input oil, this value was 23,1 MJ/kg for the HP, whereas for the upgraded oils the HHV increased up to 31.18 MJ/kg in the case of Ni/SiO_2. Significant differences were found for Ni/SiO_2 and Ni/ZrO_2 in comparison with the NiCu catalysts, that is, only between $NiCu/SiO_2$ and $NiCu/ZrO_2$ no significant differences were detected. As for the pH values, there were no considerable differences identified between the feed and the upgraded oils, and among the studied catalysts.

When analyzing the density values, it can be seen that it decreases after the hydrotreatment. The upgraded bio-oil reduces from 1.19 g/cm^3 to values between 1.09 and 1.12 g/cm^3. The upgraded oil over $NiCu/SiO_2$ displayed the lowest density (1.09 g/cm^3), while the highest corresponded to Ni/ZrO_2 (1.12 g/cm^3).

All these results give evidence of how the quality of the pyrolysis oil is clearly improved after going through the HDO reactions, indicating that this method is appropriate to obtain a biofuel of enhanced performance.

The elemental composition of the upgraded bio-oils over the four different Ni-based catalysts can be seen in Table 6 as well. The upgraded bio-oil over Ni/SiO_2 showed the highest carbon content (73.15 wt.% in dry basis, 69.75 wt.% in wet basis), while the values for the rest of the catalysts remained around 72.25 wt.% in dry basis and 67.38 wt.% in wet basis. These results are significantly higher than for the original beech wood bio-oil (54.3 wt.% in wet basis for the HP)[53]. H and N contents were very similar for all catalysts, but slightly higher in the upgraded oil in comparison to the initial feed. However, O content showed stark differences among them. The upgraded oil over Ni/SiO_2 had the lowest proportion of O (17.86 wt.% in dry basis, 21.30 wt.% in wet basis), followed by $NiCu/SiO_2$ (19.00 wt.% in dry basis, 24.10 wt.% in wet basis), Ni/ZrO_2 (19.46 wt.% in dry basis, 23.00 wt.% in wet basis) and $NiCu/ZrO_2$ (20.35 wt.% in dry basis, 23.60 wt.% in wet basis). The HP of the beech wood bio-oil had an initial O content of 38.2 wt.% in wet basis, and so it is evident that a considerable amount of O is removed during the HDO reaction, improving the quality of the original oil.

The mass balance displayed major contrasts among the tested catalysts. Ni/SiO_2 showed the highest proportion of upgraded oil (49.36 wt.%) and consequently the lowest aqueous phase (35.57 wt.%). Additionally, it had the lowest amount of solids. Nevertheless, these tendencies were not that clear for the rest of the catalysts. Ni/ZrO_2 had the lowest proportion of upgraded oil (45.32 wt.%), while $NiCu/ZrO_2$ had the highest proportion of aqueous phase (43.52 wt.%) and solids (0.32 wt.%). Gas was produced in the most elevated amount by Ni/ZrO_2 (4.54 wt.%) and in the lowest by $NiCu/SiO_2$ (3.56 wt.%). In conclusion, Ni/SiO_2 showed the most favorable mass balance for HDO.

Table 6: Mass balance and composition of the upgraded products from hydrotreatment of beech wood pyrolysis oil over fresh Ni-based catalysts at 325°C and 80 bar hydrogen.

	Ni/SiO_2	Ni/ZrO_2	$NiCu/SiO_2$	$NiCu/ZrO_2$
Mass balance				
Upgraded oil (wt.%)	49.36±0.07	45.32±0.03	49.03±0.03	46.39±0.04
Aqueous phase (wt.%)	35.57±0.07	42.72±0.01	41.45±0.01	43.52±0.03
Gas (wt.%)	4.29±0.06	4.540.05	3.56±0.07	3.87±0.03
Solids (wt.%)	0.23±0.11	0.31±0.06	0.31±0.73	0.32±0.29
Losses (wt.%)	10.54±0.17	7.10±0.05	5.65±0.47	5.90±0.49
Upgraded bio-oil (dry basis; wet basis)				
C (wt.%)	73.15±0.06; 69.75±0.21	72.22±0.00; 68.10±0.21	72.37±0.58; 66.80±0.85	72.15±1.01; 67.25±0.21
H (wt.%)	8.42±0.07; 8.55±0.07	8.25±0.00; 8.40±0.00	8.51±0.31; 8.70±0.28	8.55±0.31; 8.70±0.28
O (wt.%)	17.86±0.05; 21.30±0.00	19.46±0.15; 23.00±0.14	19.00±0.91; 24.10±1.13	20.35±0.00; 23.60±1.41
N (wt.%)	0.32±0.00; 0.30±0.00	0.32±0.00; 0.30±0.00	0.32±0.00; 0.30±0.00	0.32±0.00; 0.30±0.00
Physicochemical properties				
H_2O (wt.%)	4.85±0.07	5.10±0.00	7.30±0.42	5.95±0.35
HHV (MJ/kg)	31.18±0.08	30.85±0.02	29.86±0.26	30.27±0.31
pH	3.55±0.35	3.05±0.35	3.35±0.07	3.20±0.14
Density (g/cm^3)	1.11±0.01	1.12±0.01	1.09±0.01	1.11±0.01

ii. ^{1}H-NMR

Table 7 shows which chemical groups are assigned to each integration range of the ^{1}H-NMR spectra.

Table 7: Integration ranges of $_1$H-NMR spectra and their corresponding proton assignment.

Integration range of 1H-NMR spectra	Proton assignment
10.1-9.5	Aldehydes
8.5-6.0	(Hetero-)aromatics
6.0-4.3	Carbohydrates, water, O-H exchanging groups
4.3-3.0	Alcohols, ethers, alkenes
3.0-1.5	α proton to carboxylic acid or keto-groups, α proton to unsaturated groups
1.5-0.5	Alkanes

The signal for aldehydes (10.1-9.5 ppm) was absent in both phases for all catalysts. This is due to the fact that aldehydes are very reactive at relatively low temperatures and quickly hydrogenated to alcohols[60]. The main signal for the upgraded bio-oil was found in the α proton to carboxylic acid or keto-groups, α proton to unsaturated groups (3.0-1.5 ppm), with a concentration of 37.7 mmol/g sample, while for the aqueous phase the main signal was found in the carbohydrates, water, O-H exchanging groups (6.0-4.3 ppm), with 89.7 mmol/g sample, indicating the removal of water from the bio-oil[67]. The aromatics group (8.5-6.0 ppm) were mostly concentrated in the upgraded bio-oil and almost absent in the aqueous phase (7.2 vs. 0.8 mmol/g sample), as found by Boscagli et al.[67]. Alkenes, alcohols and ethers (4.3-3.0 ppm) were more abundant in the upgraded bio-oil (14.2 mmol/g sample) than in the aqueous phase (9.3 mmol/g sample). The abundance of alkanes (1.5-0.5 ppm) was significantly higher in the upgraded bio-oil than in the aqueous phase (20.3 vs. 2.4 mmol/g sample).

According to Mortensen at al. [11], highly reactive compounds deteriorate the quality of the bio-oil. For example, olefins have a tendency to repolymerizate in the presence of air, while ketones, aldehydes and organic acids can react to form ethers, acetales and hemiacetales. This leads to the increase of the average molecular mass of the bio-oil, its viscosity and water content.

When comparing the spectra between the feed (BWBO) and the upgraded bio-oil, the quality of the HDO reaction can be assessed. It can be clearly observed how the water content decreases in the upgraded oils (Figure 6), while the concentration of alkanes almost triplicates the one of the feed. The abundance of α proton to carboxylic acid or keto-groups, α proton to unsaturated groups is also significantly higher in the upgraded oil. Moreover, a slight increasing tendency could be observed for the concentration of alcohols, ethers and alkenes, although it was not significant for all tested catalysts. On the other hand, it is evident that the water removed from the feed is located in the aqueous phase, as it can be seen in Figure 7: all the upgraded bio-oil samples showed an increased abundance of carbohydrates, water, O-H exchanging groups in contrast to the feed. There was a small reduction in the concentration of alcohols, ethers and alkenes, as well as α proton to carboxylic acid or keto-groups, α proton to unsaturated groups. No significant differences were found for the concentration of alkanes in the aqueous phase.

In the case of the upgraded bio-oils (Figure 6), there were no significant differences among catalysts for the concentration of aromatics. Additionally, $NiCu/SiO_2$ displayed a higher amount of water content when contrasted to Ni/SiO_2 and Ni/ZrO_2, which presented the lowest values. Both $NiCu/SiO_2$ and $NiCu/ZrO_2$ showed more elevated concentrations of alcohols, ethers and alkenes than Ni/SiO_2, but they were not significantly different from Ni/ZrO_2. For the production of α proton to carboxylic acid or keto-groups, α proton to unsaturated groups , only $NiCu/ZrO_2$ differed significantly from $NiCu/SiO_2$, presenting a higher concentration. Even if Ni/ZrO_2 showed the greatest value for this group, it was not meaningful. As for alkanes, Ni/ZrO_2, $NiCu/SiO_2$ and $NiCu/ZrO_2$ were not different among them, but against Ni/SiO_2 they displayed a slightly more elevated concentration.

As for the aqueous phases (Figure 7), Ni/SiO_2 showed significantly larger water content when compared to $NiCu/SiO_2$, a clear sign of its good HDO activity. For the production of alcohols, ethers and alkenes, $NiCu/SiO_2$ presented the greatest value, followed by Ni/SiO_2, $NiCu/ZrO_2$ and Ni/ZrO_2. This last catalyst also displayed the highest amount of α proton to carboxylic acid or keto-groups, α proton to unsaturated groups in the aqueous phase, while the remaining three catalysts did not show significant differences among them. With very small differences, $NiCu/SiO_2$ had the most elevated abundance of alkanes, followed by $NiCu/ZrO_2$, Ni/ZrO_2 and Ni/SiO_2.

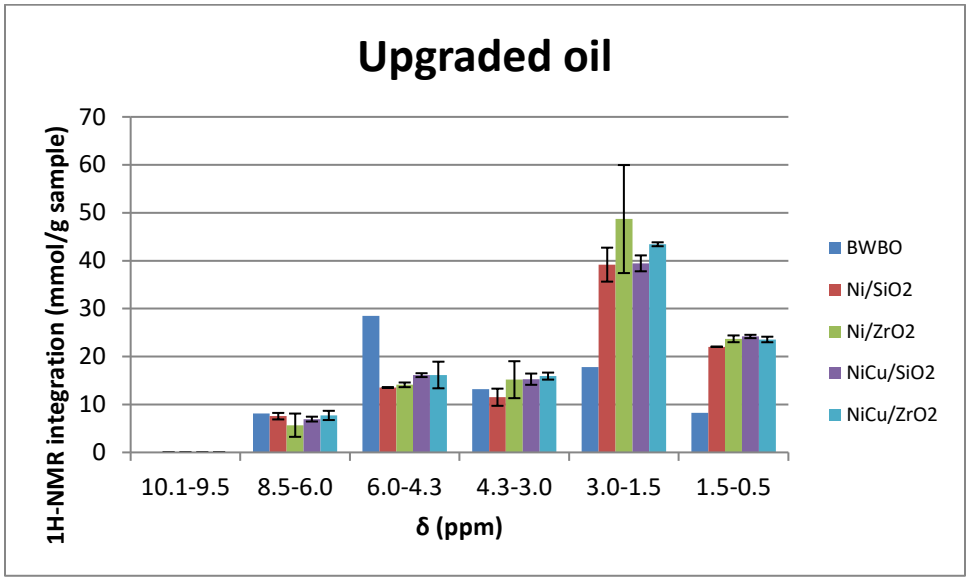

Figure 6: Integration of ^{1}H-NMR spectra of the upgraded oil produced from HDO of beech wood bio-oil over fresh Ni/SiO_2, Ni/ZrO_2, $NiCu/SiO_2$ and $NiCu/ZrO_2$, with the feed as reference (BWBO).

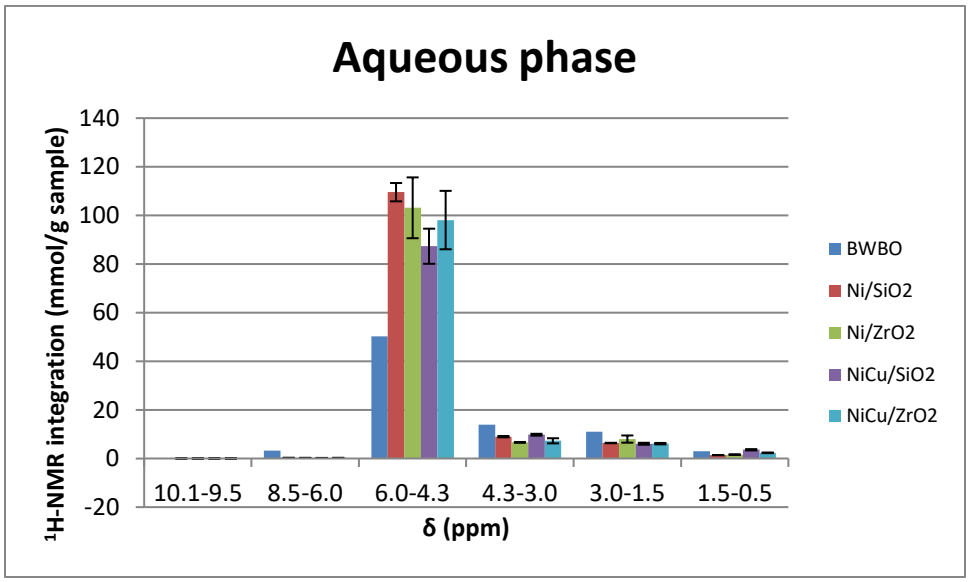

Figure 7: Integration of ^{1}H-NMR spectra of the aqueous phase produced from HDO of beech wood bio-oil over fresh Ni/SiO_2, Ni/ZrO_2, NiCu/SiO_2 and NiCu/ZrO_2, with the feed as reference (BWBO).

iii. GC-FID

Considering the consumption of hydrogen, NiCu/SiO_2 presented the highest volume (239.3 NL/kg bio-oil), followed by NiCu/ZrO_2 (201.6 NL/kg bio-oil), Ni/SiO_2 (186.2 NL/kg bio-oil) and Ni/ZrO_2 (181.9 NL/kg bio-oil). There was no significant difference between the monometallic Ni catalysts, which consumed much less hydrogen than the NiCu catalysts. As it was reported by Yin et al.[55], the addition of Cu to the monometallic Ni catalyst leads to a higher hydrogenation activity, due to significant changes in catalytic activity and selectivity. Cu can prevent the formation of carbon and the sintering of the active phase particles, while enhancing the activity of some hydrogenation reactions, such as the hydrogenation of ethylene and 1,3-butadiene [68].

NiCu/ SiO_2 had a higher hydrogen consumption than NiCu/ZrO_2. It is known that SiO_2 has a better stability, weak acidity nature and low affinity for carbon formation[32]. Additionally, ZrO_2 favors the activation of O-compounds in the support surface and also displays a low carbon deposition. Although, as it was stated in Table 2, it has been found that carbon deposition was higher in ZrO_2-supported catalysts. Moreover, the reduced surface area of ZrO_2 is unfavorable for the improvement of catalytic performance. Zhang et al.[37] added SiO_2 in order to overcome this disadvantage.

Although a very similar total gas production was seen for all tested catalysts, Ni/ZrO_2 displayed the highest total gas production (1.06 mol/kg bio-oil), followed by Ni/SiO_2 (0.99 mol/kg bio-oil), NiCu/ZrO_2 (0.9 mol/kg bio-oil) and NiCu/SiO_2 (0.86 mol/kg bio-oil). Total gas production was mainly determined by the production of CO_2, which was the most abundant gas product for all four catalysts. This results were also obtained by other authors[63,67,69,70]. CO_2 is formed by decarboxylation of carboxylic acids or redox reactions among organic molecules involving also

water. The other more abundant produced gases were CO and methane, while gases such as propane, propene, ethane and ethene were formed in very small amounts.

Monometallic Ni catalysts produced the highest amount of CO_2, followed by $NiCu/ZrO_2$ and later by $NiCu/SiO_2$. According to Gallakota et al. [23], the generation of CO_2 is a sign of low HDO activity: 100% of carbon effectiveness means all C atoms are converted to hydrocarbons without CO_2 flows. Nevertheless, what must be taken into account is that, as the total gas production of the four catalysts represents around 4 wt.% (see mass balance table above), the produced amounts of CO_2 are in general quite reduced in these four cases. Elevated CO_2 formation indicates reduced deoxygenation via H_2O formation and thus reduced hydrogen consumption, though CO_2 also indicates a loss in oil yield [71]. This effect was observed when the CO_2 production was compared to the hydrogen consumption: both variables are inversely proportional, as it has also been reported by Boscagli et al.[67]. This tendency was only found in CO_2 production, but not for the remaining produced gases.

The formation of methane was higher in $NiCu/SiO_2$, followed by Ni/ZrO_2, $NiCu/ZrO_2$ and Ni/SiO_2. Methane could be formed by demethylation of methoxy groups; the competing transalkylation reaction which would retain carbon in the oil fraction typically requires acid sites. Other reported routes include hydrogenation of carbohydrates, decomposition of acetic acid or C-C cleavage from higher alcohols. Methane formation is associated with both reduction in carbon yield and hydrogen consumption[71].

CO formation was more abundant in the SiO_2-supported catalysts: $NiCu/SiO_2$ displayed the highest amount, followed by Ni/SiO_2, Ni/ZrO_2 and $NiCu/ZrO_2$. One pathway to form CO could be C-O cleavage from aldehydes, alcohols or acids. CO presents a loss of C, as well as CO_2, though at the same time it may indicate a reduction in hydrogen consumption. The loss of C via CO, called decarbonylation, is less advantageous than the loss via CO_2, known as decarboxylation. This is due to the fact that more O is removed per mole of lost carbon. Compared to dehydration, no hydrogen is consumed or more hydrogen is retained in the oil[71].

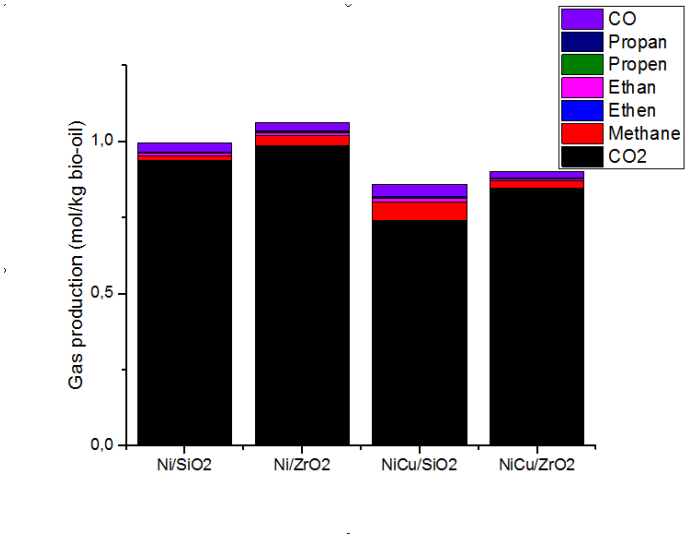

Figure 8: Gas production during the HDO over different Ni-based catalysts (325°C, 80 bar hydrogen at room temperature).

iv. ICP-OES

ICP-OES was further used to evaluate the metal content present in the aqueous phase once the HDO reaction was performed. With the obtained results, metal leaching was calculated.

Table 8: Concentration of metals leached to the aqueous phase after HDO over different Ni-based catalysts (325°C, 80 bar hydrogen at room temperature).

Metal concentration (µg/ml)	Ni	Cu
Ni/SiO_2	79.0	-
Ni/ZrO_2	36.4	-
$NiCu/SiO_2$	50.2	2.7
$NiCu/ZrO_2$	49.6	1.0

To calculate the proportion of active metals that were washed to the aqueous phase, the amount of metal in the freshly synthesized catalyst in µg was calculated using the metal concentration obtained in the ICP analysis of the catalysts (see Table 4). Later on, with the concentration of the metal in the aqueous phase (Table 8) and the density values of the aqueous phase, the amount of leached metal per mass unit of aqueous phase (µg metal/g LP) was calculated. This result divided by the amount of metal in the fresh catalyst and multiplied by the mass of aqueous phase obtained after the HDO reaction derives in the proportion of metal that is leached to the aqueous phase.

Leaching levels for the four tested catalysts at the prevailing reaction conditions were very low. Ni/SiO_2 presented 0.8% of Ni leached to the aqueous phase, while Ni/ZrO_2 had a 0.43% of its Ni

content washed to this oil fraction. Moreover, NiCu catalysts showed the same leaching level for Ni: 0.16%. As for Cu, NiCu/SiO_2 displayed 0.08% of leaching, while NiCu/ZrO_2 had 0.04%.

Generally speaking, no significant leaching was detected for the active metals in study. This could be explained by the reducing reaction atmosphere created by the reaction, which stabilizes Ni in the metallic form. Similar leaching levels were also found by Boscagli et al. for a reaction temperature of 240°C over a NiCu/Al_2O_3 catalyst[40]. As the HDO reactions are performed at severe conditions (325°C for 2 hours, including the presence of water near critical conditions and organic acids), the structure, morphology and texture of the catalysts may be affected[69]. The extent of leaching is strongly related to the type of support that is being used for the catalyst: ZrO_2-supported catalysts showed lower proportions of leached metal than SiO_2-supported catalysts, although this difference was more noticeable for the monometallic Ni catalysts. As it was reported by some authors, ZrO_2 is more stable at the reaction conditions than other types of supports[35,36,69,72].

c. Catalyst regeneration

Once the original reactions with the fresh catalyst were carried out, the catalyst with the best performance had to be chosen. To do so, several characteristics of the produced upgraded oil and the catalyst were taken into account. For example, the carbon, O and water contents of the resulting upgraded bio-oil and the amount of hydrogen consumed during the reaction for each catalyst. These results can be observed in Table 5 and Figure 11. The upgraded oil produced when using Ni/SiO_2 as catalyst displays the highest carbon content and the lowest O content when compared to the rest of the catalysts. These two characteristics indicate an enhancement in oil quality, such as a higher energy density and a better chemical stability of the fuel. Additionally, Ni/SiO_2 showed the second lowest hydrogen consumption after Ni/ZrO_2, which is a sign of high efficiency in the HDO. The water content in the oil produced with Ni/SiO_2 was the lowest, indicating as well a satisfying HDO performance.

Additionally, Ni/SiO_2 presented the lowest sulfur deposition (Table 4), the lowest amount of solids, the highest yield in upgraded bio-oil, HHV and pH (Table 5). Finally, it also produced the smallest amount of methane (Figure 8). Therefore, Ni/SiO_2 was selected to carry out the three following regeneration steps.

i. Evaluation of catalyst performance during the regeneration cycles

Considering that Ni/SiO_2 had been selected for further investigation in HDO regeneration cycles, a detailed characterization, which is presented in this section, was made for each intermediate step of the process: spent, calcined and reduced forms

After each regeneration step, the spent Ni/SiO_2 was evaluated using the SEM-EDX technique (Table 9). ICP could have been also used, but the amount of samples was too low. Small amounts of sulfur near the detection limit appeared on the surface of the catalyst, indicating a low level of poisoning in the material. It is interesting to highlight that this concentration did not increase

along the regeneration steps, which would have been the expected tendency. Additionally, carbon deposition increased dramatically when comparing the spent forms from the original reaction with the first regeneration (13.8 wt.% vs. 43.9 wt.%). However, this value decreased in the second regeneration and increased again in the third. In this case, no clear trend could be identified, though in average the carbon deposition was significantly higher in the regeneration steps than in the original reaction (20.4 wt.% vs. 13.8 wt.%). Furthermore, the concentration of Ni in the spent catalyst was significantly decreased from the original reaction to the regeneration steps, which shows how the carbon deposits and the poisoning elements negatively affect the amount of active sites in the catalyst. As for the carbon deposition, no trend could be identified for the concentration of Ni on the catalyst surface. This eclectic behavior could be due to the fact that EDX measurements can be made either as element mapping or point analysis[73]. In this study, both methods were used, and consequently different locations in the catalyst surface were analyzed. As this surface is not homogeneous, each evaluated point differs from the others, and so significantly contrasting results can be obtained.

Table 9: Concentration of elements present on the surface of Ni/SiO_2 in its spent form after HDO in its first, second and third regeneration (325°C, 80 bar hydrogen at room temperature).

Catalyst	Form	Ni (wt%)	Si (wt%)	O (wt%)	C (wt%)	S (wt%)
Ni/SiO_2	1st regeneration	1.6	22.1	32.1	43.9	0.1
	2nd regeneration	2.8	42.2	48.5	6.2	0.1
	3rd regeneration	1.5	40.2	46.9	11.2	0.1

Furthermore, the catalyst was analyzed using XRD for each regeneration cycle, in the spent, calcined and reduced forms. In the case of the spent form in the first regeneration (Figure 12), metallic Ni was identified. After the calcination, the reflections for metallic Ni disappears and the reflection for NiO is visible. In the reduced form, the reflections for NiO disappear, leaving just the peaks for metallic Ni and the support left.

In other works[40], Ni_3S_2 (an alloy between Ni and S) had been identified at 31.1° in the HDO of pyrolysis oil over $NiCu/Al_2O_3$ corresponding to the (110) plane of Ni_3S_2[74,75]. In the current study, the concentration of S in the catalyst was too small to identify such substance.

In the consecutive regenerations, that is second and third (Figures 13 and 14), the behavior of the catalyst remains unchanged. Apart from the signal of the support, only metallic Ni can be found in the spent form. In the calcined form, the reflection for NiO is again identified, with no metallic Ni present. Once the catalyst is reduced, the oxidized form of the metal vanishes and only metallic Ni is remaining.

Additionally, the crystallite sizes were evaluated after each regeneration. A tendency of increasing crystallite size could be observed, as it was also identified by other authors[40]: the freshly reduced Ni/SiO_2 catalyst had a size of 17.7 nm, which later increased to 21.05 nm after the reaction. For the subsequent regenerations, the crystallite size increased steadily, reaching a maximum value of

37.3 nm after the last regeneration, indicating a significant particle agglomeration and sintering occurring after each reaction[60].

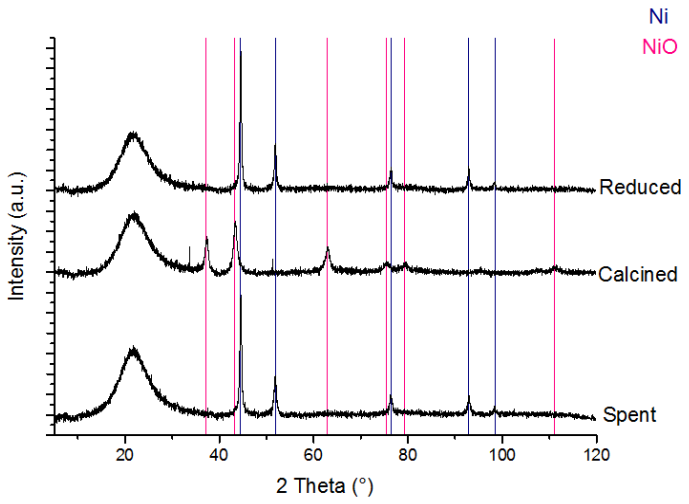

Figure 12: Diffractogram from the selected Ni/SiO_2 catalyst for its first regeneration in its spent, calcined and reduced forms.

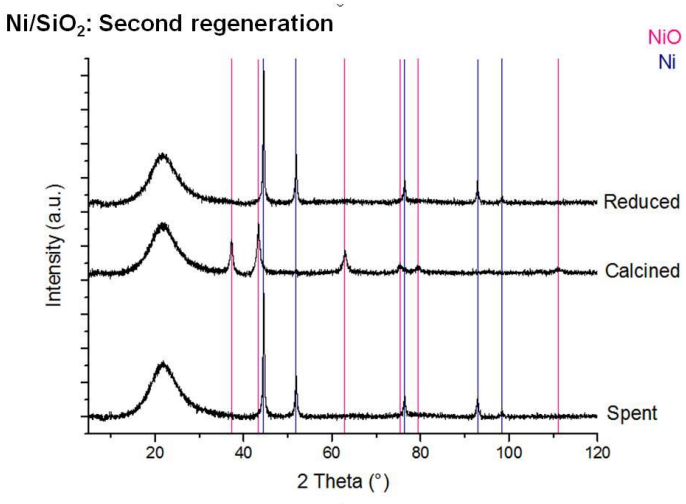

Figure 13: Diffractogram from the selected Ni/SiO_2 catalyst for its second regeneration in its spent, calcined and reduced forms.

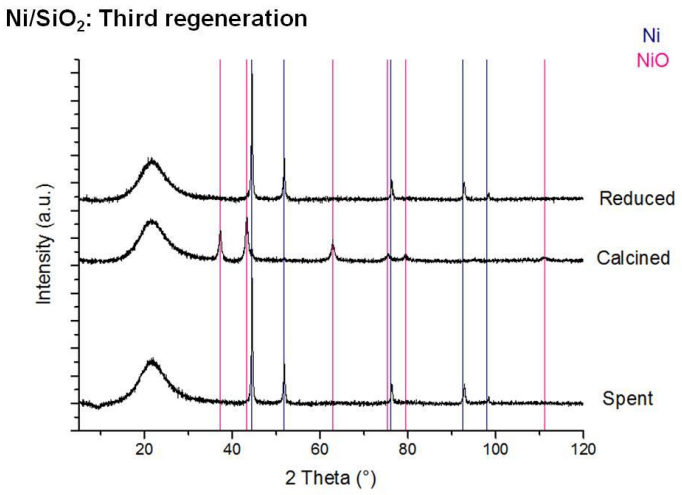

Figure 14: Diffractogram from the selected Ni/SiO_2 catalyst for its third regeneration in its spent, calcined and reduced forms.

The BET surface area was measured for the spent catalyst after the third regeneration. The freshly synthesized catalyst had a surface area of 214.7 m^2/g of catalyst, which was reduced to 46.1 m^2/g after the first use and later to 38.8 m^2/g after the third regeneration step (spent catalyst). The decrease was less marked after the first use of the catalyst, probably because when the quality of the support is maintained, the active phase of the catalyst may also be in good conditions[15].

ii. Characterization of upgraded products

The upgraded bio-oils were analyzed after each regeneration step. Their elemental analysis was performed and their main physicochemical properties were measured. In Table 10, it can be observed how the carbon content decreases along the regenerations, more sharply between the first and the second. In addition, the O content increases, reaching a 20.35 wt.% after the third regeneration of the catalyst. Water content also rises, although in smaller measure when compared to the O content.

No significant variations could be observed for the HHV as well as the pH values. The stability of the pH could be directly linked to the abundance of carboxylic acids, which will be assessed later on in this study: if the concentration of carboxylic acids does not change, the pH will remain unmodified. A trend of increasing oil density with increasing number of regenerations may be possible to identify, but data for the second and third regenerations were not available.

Similar tendencies were found by Boscagli et al.[40] when evaluating the performance of regenerated catalysts, although in their study only one regeneration was considered. Apart from the previously mentioned results, they also observed a decrease in hydrogen consumption: there was a reduction of 17.18% in the consumption of hydrogen between the original reaction and the first regeneration, 6.28% between the first and the second, and just 0.66% between the second

and third regenerations. This drop in the consumption of hydrogen indicates a decline in the HDO activity. Additionally, an increase in the total gas production was found, which could be mainly due to the occurrence of more cracking reactions.

Table 10: Physicochemical properties and elemental analysis (in dry basis) of the upgraded bio-oil, hydrogen consumption and total gas production after the original reaction and the first, second and third catalyst regenerations.

Property	Original	1st regeneration	2nd regeneration	3rd regeneration
C (wt.%)	73.15	73.54	72.37	72.15
H (wt.%)	8.42	8.25	8.51	8.55
O (wt.%)	17.86	17.74	19.00	20.35
N (wt.%)	0.32	0.32	0.32	0.32
H_2O (wt.%)	4.85	5.4	5.5	5.3
HHV (MJ/kg)	31.18	30.92	31.11	31.26
pH	3.6	2.8	3.5	3.4
Density (g/cm^3)	11.135	11.261	n.b.	n.b.
H_2 consumption(NL/kg)	186.21	154.22	144.53	143.58
Gas production (mol/kg)	0.99	1.23	1.31	1.35

^{1}H-NMR was also performed for the upgraded bio-oils and the aqueous phases obtained over the regenerated catalysts.

The signal for aldehydes (10.1-9.5 ppm) was absent in both phases for all regeneration stages. As it was exposed earlier, aldehydes are very reactive at relatively low temperatures and quickly hydrogenated to alcohols[60]. The highest signal for the upgraded bio-oil was found in the α protons to unsaturated, carboxylic acids and keto-groups (3.0-1.5 ppm) with an average value among regenerations of 39.4 mmol/g sample, while for the aqueous phase it was located in the water, O-H exchanging groups and carbohydrates group (6.0-4.3 ppm), with an average of 95.2 mmol/g sample. The production of aromatics (8.5-6.0 ppm) was mostly concentrated in the upgraded bio-oil and almost absent in the aqueous phase (9.4 mmol/g sample vs. 0.2 mmol/g sample in average). The production of alkenes, alcohols and ethers (4.3-3.0 ppm) were concentrated in the upgraded bio-oil (10.4 mmol/g sample in upgraded bio-oil vs. 5.7 mmol/g sample in aqueous phase in average). Alkanes (1.5-0.5 ppm) were highly abundant in the upgraded bio-oil in contrast to the aqueous phase (23.3 mmol/g sample vs. 1.1 mmol/g sample in average).

Within the upgraded bio-oil, it could be seen that aromatics increased in the first regeneration in contrast to the original upgrading reaction, but later dropped in the subsequent regeneration steps. A similar trend was observed for the carbohydrates, water and O-H exchanging groups, which was in accordance to the increase in water content in the upgraded bio-oils of the upgraded oil (Table 10). A small decrease in the abundance of alcohols, ethers and alkenes, as well as the α proton to unsaturated groups could be seen, although the latter showed a dramatic increase in

the first regeneration and declined slightly below the levels of the original upgrading reaction in the following two regeneration steps. This increase in the first regeneration was reflected in the pH value of the upgraded oil, which presented a value of 2.8. For the aldehydes group, no clear tendency could be found, as its concentration remained quite stable along the regenerations (Figure 15).

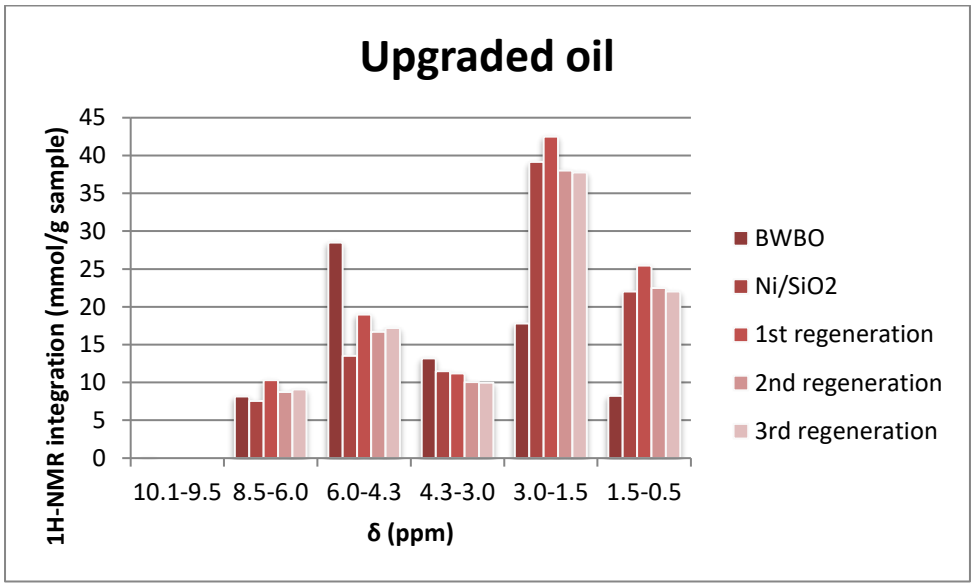

Figure 15: Integration of ^{1}H-NMR spectra of the upgraded oil produced from HDO of beech wood bio-oil over original Ni/SiO_2 catalyst, and the following three regenerations, with the feed as reference (BWBO).

On the other hand, within the aqueous phase, the opposite tendency was observed for the carbohydrates, water and O-H exchanging groups: a decline along the regenerations was seen, probably because of the higher water content in the upgraded bio-oil (Figure 16). The signal for alcohols, ethers and alkenes also dropped, from a value of 8.66 mmol/g sample after the original reaction to 5.19 mmol/g sample after the third regeneration. The signals for α proton to carboxylic acid or keto-groups, α proton to unsaturated groups and for alkanes displayed a very small reduction along the regeneration steps, almost remaining unchanged after each reutilization of the catalyst.

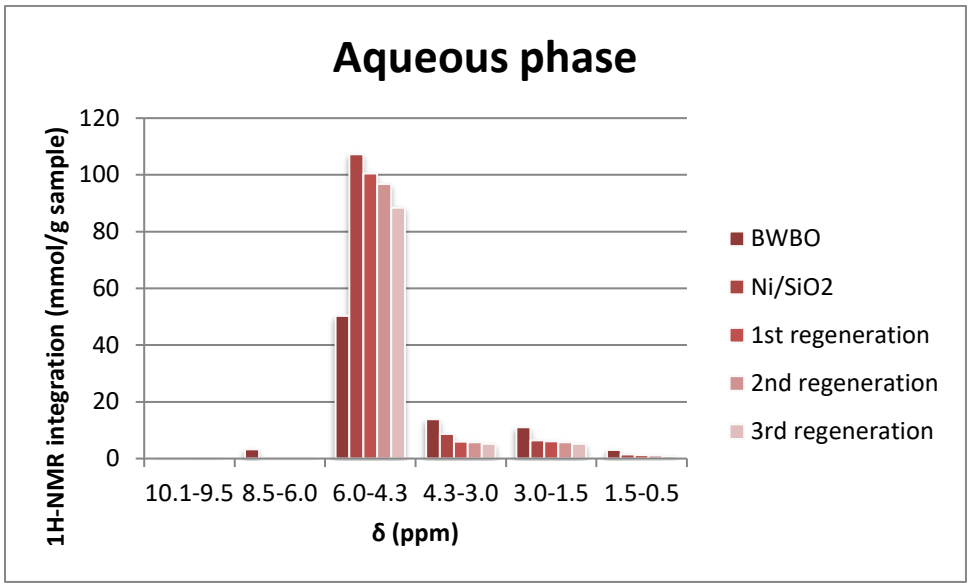

Figure 16: Integration of ^{1}H-NMR spectra of the aqueous phase produced from HDO of beech wood bio-oil over original Ni/SiO_2 catalyst, and the following three regenerations, with the feed as reference (BWBO).

7. Conclusion

In this work, four Ni-based catalysts were evaluated for the HDO of beech wood pyrolysis oil. After being synthesized, their superficial and compositional characteristics were assessed. Once the upgrading reaction was performed for the pyrolysis oil, the resulting products (upgraded bio-oil, aqueous phase and gas fraction) were separately analyzed. Considering the obtained results, the catalyst with the best upgrading performance was selected in order to regenerate and use it in further HDO reactions. The catalyst selection was based on upgraded bio-oil, catalyst and reaction factors. The upgraded bio-oil obtained over Ni/SiO_2 showed the lowest O and water contents, the highest concentration of carbon and the highest HHV and pH values. As a catalyst, Ni/SiO_2 presented the lowest S deposition on its surface. Finally, during the reaction, Ni/SiO_2 produced the smallest amount of solids, methane and consumed the least quantity of hydrogen among all catalysts.

Considering the results detailed above, Ni/SiO_2 was chosen and therefore regenerated, which included the calcination and reduction of the spent catalyst before it was reused in a new HDO reaction. Its performance was tested along three consecutive reactions. The upgraded bio-oils corresponding to the regeneration cycles displayed a decrease in the carbon content and an increase in the concentration of O and water. Nevertheless, both HHV and pH values were not affected along the regenerations. A decline in the hydrogen consumption was also observed, indicating a reduction in the HDO activity. When evaluating the catalyst performance, a small amount of S deposited on the catalyst surface could be observed, which did not increase along the cycles, in addition to a carbon deposition significantly higher in comparison to the original set of reactions.

Altogether, it can be concluded that Ni/SiO_2 improved the oil properties and showed a satisfactory performance after three regeneration cycles. This indicates that this catalyst can be regenerated and reused for a minimum of three times without significantly affecting the resulting upgraded bio-oil. Further characterization techniques, such as quantification of chemical compounds by gas chromatography-mass spectrometry/flame ionization detector (GC-MS) and distribution of molecular weight by gel permeation chromatography (GPC) should be performed in order to achieve a bigger understanding of the functioning of Ni-based catalysts and their reutilization in a larger number of consecutive upgrading reactions.

8. References

1. Kan, T., Strezov, V. & Evans, T. J. Lignocellulosic biomass pyrolysis : A review of product properties and effects of pyrolysis parameters. *Renew. Sustain. Energy Rev.* **57,** 1126–1140 (2016).

2. García-Olivares, A., Solé, J. & Osychenko, O. Transportation in a 100% renewable energy system. *Energy Convers. Manag.* **158,** 266–285 (2018).

3. Balsalobre-lorente, D., Shahbaz, M., Roubaud, D. & Farhani, S. How economic growth , renewable electricity and natural resources contribute to CO 2 emissions ? *Energy Policy* **113,** 356–367 (2018).

4. Guedes, R. E., Luna, A. S. & Torres, A. R. Operating parameters for bio-oil production in biomass pyrolysis: A review. *J. Anal. Appl. Pyrolysis* 0–1 (2017). doi:10.1016/j.jaap.2017.11.019

5. IEA. IEA Energy Technology Essentials - Biomass for Power Generation and CHP. *High Temp.* 1–4 (2007).

6. Bridgwater, A. V. Renewable fuels and chemicals by thermal processing of biomass. *Chem. Eng. J.* **91,** 87–102 (2003).

7. El Bassam, N. *Handbook of bioenergy crops. A complete reference to species, development and applications. Journal of Cleaner Production* **18,** (Earthscan, 2010).

8. Sharma, A., Pareek, V. & Zhang, D. Biomass pyrolysis — A review of modelling , process parameters and catalytic studies. *Renew. Sustain. Energy Rev.* **50,** 1081–1096 (2015).

9. Mohan, D., Pittman, C. U. & Steele, P. H. Pyrolysis of Wood / Biomass for Bio-oil : A Critical Review. 848–889 (2006). doi:10.1021/ef0502397

10. Si, Z., Zhang, X., Wang, C., Ma, L. & Dong, R. An Overview on Catalytic Hydrodeoxygenation of Pyrolysis Oil and Its Model Compounds. *Catalysts* **7,** 1–22 (2017).

11. Mortensen, P. M., Grunwaldt, J., Jensen, P. A., Knudsen, K. G. & Jensen, A. D. A review of catalytic upgrading of bio-oil to engine fuels. *"Applied Catal. A, Gen.* **407,** 1–19 (2011).

12. Song, H., Gong, J., Song, H. & Li, F. Applied Catalysis A : General A novel surface modification approach for synthesizing supported nickel phosphide catalysts with high activity for hydrodeoxygenation of benzofuran. *"Applied Catal. A, Gen.* **505,** 267–275 (2015).

13. Ewald, S., Standl, S. & Hinrichsen, O. Characterization of nickel catalysts with transient methods. *Appl. Catal. A Gen.* **549,** 93–101 (2018).

14. Olbrich, W. *et al.* Catalytic hydrodeoxygenation of pyrolysis oil over nickel - based catalysts under H 2 / CO 2 atmosphere. *Sustain. Chem. Process.* **4,** 1–8 (2016).

15. Dufresne, P. Hydroprocessing catalysts regeneration and recycling. **322,** 67–75 (2007).

16. Ng, A., Lup, K., Abnisa, F., Mohd, W. & Wan, A. A review on reactivity and stability of heterogeneous metal catalysts for deoxygenation of bio-oil model compounds. *J. Ind. Eng. Chem.* **56,** 1–34 (2017).

17. Kanaujia, P. K., Sharma, Y. K., Agrawal, U. C. & Garg, M. O. Analytical approaches to characterizing pyrolysis oil from biomass. *Trends Anal. Chem.* **42,** 125–136 (2013).

18. Rezaei, P. S., Shafaghat, H. & Daud, W. M. A. W. Production of green aromatics and olefins by catalytic cracking of oxygenate compounds derived from biomass pyrolysis: A review. *Appl. Catal. A Gen.* **469,** 490–511 (2014).

19. Demirbas, A. The influence of temperature on the yields of compounds existing in bio-oils obtained from biomass samples via pyrolysis. *Fuel Process. Technol.* **88,** 591–597 (2007).

20. Czernik, S., Johnson, D. K. & Black, S. Stability of wood fast pyrolysis oil. *Biomass and Bioenergy* **7,** 187–192 (1994).

21. Li, X. *et al.* Upgrading of bio-oil into advanced biofuels and chemicals. Part III. Changes in aromatic structure and coke forming propensity during the catalytic hydrotreatment of a fast pyrolysis bio-oil with Pd/C catalyst. *Fuel* **116,** 642–649 (2014).

22. Yang, H., Yao, J. & Chen, G. Overview of upgrading of pyrolysis oil of biomass. *Energy Procedia* **61,** 1306–1309 (2014).

23. Gollakota, A. R. K., Reddy, M., Subramanyam, M. D. & Kishore, N. A review on the upgradation techniques of pyrolysis oil. *Renew. Sustain. Energy Rev.* **58,** 1543–1568 (2016).

24. Balat, M. An overview of the properties and applications of biomass pyrolysis oils. *Energy Sources, Part A Recover. Util. Environ. Eff.* **33,** 674–689 (2011).

25. Furimsky, E. Catalytic hydrodeoxygenation. **199,** 147–190 (2000).

26. Wildschut, J., Mahfud, F. H., Venderbosch, R. H. & Heeres, H. J. Hydrotreatment of Fast Pyrolysis Oil Using Heterogeneous Noble-Metal Catalysts. 10324–10334 (2009).

27. Cecilia, J. A., Infantes-Molina, A. & Rodríguez-Castellón, E. Oxygen-removal of dibenzofuran as a model compound in biomass derived bio-oil on nickel phosphide catalysts: Role of phosphorus. *"Applied Catal. B, Environ.* **136–137,** 140–149 (2013).

28. Elliott, D. C. Biofuel from fast pyrolysis and catalytic hydrodeoxygenation. *Curr. Opin. Chem. Eng.* **9,** 59–65 (2015).

29. Jin, S. *et al.* Catalytic hydrodeoxygenation of anisole as lignin model compound over supported nickel catalysts. *Catal. Today* **234,** 125–132 (2014).

30. Yang, Y., Chen, J. & Shi, H. Deoxygenation of methyl laurate as a model compound to hydrocarbons on Ni2P/SiO2, Ni2P/MCM-41, and Ni2P/SBA-15 catalysts with different dispersions. *Energy and Fuels* **27,** 3400–3409 (2013).

31. Li, Y. *et al.* Coke formation on the surface of Ni / HZSM-5 and Ni-Cu / HZSM-5 catalysts during bio-oil hydrodeoxygenation. **189,** 23–31 (2017).

32. He, Z. & Wang, X. Hydrodeoxygenation of model compounds and catalytic systems for pyrolysis bio-oils upgrading. *Catal. Sustain. Energy* (2012). doi:10.2478/cse-2012-0004

33. Oh, S., Choi, H. S., Choi, I.-G. & Choi, J. W. Evaluation of hydrodeoxygenation reactivity of pyrolysis bio-oil with various Ni-based catalysts for improvement of fuel properties. *RSC Adv.* **7,** 15116–15126 (2017).

34. Zhao, H. Y., Li, D., Bui, P. & Oyama, S. T. Hydrodeoxygenation of guaiacol as model compound for pyrolysis oil on transition metal phosphide hydroprocessing catalysts. *Appl. Catal. A Gen.* **391,** 305–310 (2011).

35. Ardiyanti, A. R., Gutierrez, A., Honkela, M. L., Krause, A. O. I. I. & Heeres, H. J. Hydrotreatment of wood-based pyrolysis oil using zirconia-supported mono- and bimetallic (Pt , Pd , Rh) catalysts. *"Applied Catal. A, Gen.* **407,** 56–66 (2011).

36. He, Z. & Wang, X. Hydrodeoxygenation of model compounds and catalytic systems for pyrolysis bio-oils upgrading. *Catal. Sustain. energy* 28–52 (2012). doi:10.2478/cse-2012-0004

37. Zhang, X. *et al.* Characterization and catalytic properties of Ni and NiCu catalysts supported on ZrO2-SiO2 for guaiacol hydrodeoxygenation. *Catal. Commun.* **33,** 15–19 (2013).

38. De, M. Catalyst Science and Technology Course. *National Programme on Technology Enhanced Learning (NPTEL) - Phase II* (2014).

39. Jones, M. N. Milde Hydrodeoxygenierung eines Pyrolyseligninmodells an einem Nickel-

basierten Katalysator. (2015).

40. Boscagli, C. *et al.* Effect of pyrolysis oil components on the activity and selectivity of catalysts during hydrotreatment. *"Applied Catal. A, Gen.* **544,** 161–172 (2017).

41. Moulijn, J. A., van Leeuwen, P. W. N. M. & van Santen, R. A. *Chapter 10: Catalyst characterization with spectroscopic techniques*. *Studies in Surface Science and Catalysis* **79,** (1988).

42. Patterson, A. L. The Scherrer Formula for X-Ray Particle Size Determination. *Phys. Rev.* **56,** 978–982 (1939).

43. Boscagli, C., Raffelt, K., Zevaco, T. A., Olbrich, W. & Otto, T. N. Mild hydrotreatment of the light fraction of fast-pyrolysis oil produced from straw over nickel-based catalysts. *Biomass and Bioenergy* **83,** 525–538 (2015).

44. Krosse, S. & van der Ven, P. Elemental analysis/amino-acids: ICP-OES. *General Instrumentation. Faculty of Science. Radboud University.* (2018). Available at: http://www.ru.nl/science/gi/facilities-activities/elemental-analysis/icp-oes/. (Accessed: 9th April 2018)

45. Friedl, A., Padouvas, E., Rotter, H. & Varmuza, K. Prediction of heating values of biomass fuel from elemental composition. *Anal. Chim. Acta* **544,** 191–198 (2005).

46. Kaseman, D. & Iyer, R. S. G. Magnetic Resonance Spectroscopies: Nuclear Magnetic Resonance. *Chemistry LibreTexts* (2017).

47. Roldugina, E. A., Naranov, E. R., Maximov, A. L. & Karakhanov, E. A. Hydrodeoxygenation of guaiacol as a model compound of bio-oil in methanol over mesoporous noble metal catalysts. *"Applied Catal. A, Gen.* (2018). doi:10.1016/j.apcata.2018.01.008

48. Esmaeili, J. & Rahimpour, F. Regeneration of spent nickel catalyst from hydrogenation process of edible oils : Heat treatment with hydrogen injection. *Int. J. Hydrogen Energy* **42,** 24197–24204 (2017).

49. Bykova, M. V *et al.* Applied Catalysis B : Environmental Ni-based sol – gel catalysts as promising systems for crude bio-oil upgrading : Guaiacol hydrodeoxygenation study. *"Applied Catal. B, Environ.* **113–114,** 296–307 (2012).

50. Rogatis, L. De, Montini, T., Cognigni, A., Olivi, L. & Fornasiero, P. Methane partial oxidation on NiCu-based catalysts. **145,** 176–185 (2009).

51. Bykova, M. V. *et al.* Ni-based sol-gel catalysts as promising systems for crude bio-oil

upgrading: Guaiacol hydrodeoxygenation study. *Appl. Catal. B Environ.* **113–114,** 296–307 (2012).

52. Ardiyanti, A. R. *Hydrotreatment of fast pyrolysis oil Hydrotreatment of Fast Pyrolysis Oil Catalyst Development and Process-Product Relations*. (2013).

53. Carriel Schmitt, C., Boscagli, C., Rapp, M., Raffelt, K. & Dahmen, N. Characterization of light and heavy phase of pyrolysis-oil from distinct biomass for further upgrading reactions. doi:10.5071/25thEUBCE2017-3AV.3.15

54. Koike, N. *et al.* Upgrading of pyrolysis bio-oil using nickel phosphide catalysts. **333,** 115–126 (2016).

55. Yin, W. *et al.* Hydrotreatment of the carbohydrate-rich fraction of pyrolysis liquids using bimetallic Ni based catalyst : Catalyst activity and product property relations. **169,** 258–268 (2018).

56. Rodríguez, J. C., Marchi, A. J., Borgna, A., Romeo, E. & Monzón, A. Gas Phase Selective Hydrogenation of Acetylene. Importance of the Formation of Ni-Co and Ni-Cu Bimetallic Clusters on the Selectivity and Coke Deposition. *Stud. Surf. Sci. Catal.* **139,** 37–44 (2001).

57. De Rogatis, L., Montini, T., Lorenzut, B. & Fornasiero, P. NixCuy/Al2O3 based catalysts for hydrogen production. *Energy Environ. Sci.* **1,** 501–509 (2008).

58. Ardiyanti, A. R., Khromova, S. A., Venderbosch, R. H., Yakovlev, V. A. & Melián-cabrera, I. V. Catalytic hydrotreatment of fast pyrolysis oil using bimetallic Ni – Cu catalysts on various supports. *Appl. Catal. A Gen.* **449,** 121–130 (2012).

59. Haasterecht, T. Van, Ludding, C. C. I., Jong, K. P. De & Bitter, J. H. Toward stable nickel catalysts for aqueous phase reforming of biomass-derived feedstock under reducing and alkaline conditions. *J. Catal.* **319,** 27–35 (2014).

60. Yin, W. *et al.* Catalytic hydrotreatment of fast pyrolysis liquids in batch and continuous set-ups using bimetallic Ni-Cu catalyst with a high metal content. *Catal. Sci. Technol.* **6,** 5899–5915 (2016).

61. Whiffen, V. M. L. & Smith, K. J. Hydrodeoxygenation of 4-methylphenol over unsupported MoP, MoS2, and MoOx catalysts. *Energy and Fuels* **24,** 4728–4737 (2010).

62. Stichert, W. & Schüth, F. Influence of crystallite size on the properties of zirconia. *Chem. Mater.* **10,** 2020–2026 (1998).

63. Wang, Z., Zeng, Y., Lin, W. & Song, W. In-situ hydrodeoxygenation of phenol by supported

Ni catalyst – explanation for catalyst performance. *Int. J. Hydrogen Energy* **42,** 21040–21047 (2017).

64. Chen, S. *et al.* Study of catalytic hydrodeoxygenation performance of Ni catalysts : Effects of prepared method. *Renew. Energy* **115,** 1109–1117 (2018).

65. Oh, S., Hwang, H., Seok, H. & Weon, J. The effects of noble metal catalysts on the bio-oil quality during the hydrodeoxygenative upgrading process. *FUEL* **153,** 535–543 (2015).

66. Li, X. *et al.* Heterogeneous sulfur-free hydrodeoxygenation catalysts for selectively upgrading the renewable bio-oils to second generation biofuels. *Renew. Sustain. Energy Rev.* **82,** 3762–3797 (2018).

67. Boscagli, C., Raffelt, K. & Grunwaldt, J. Reactivity of platform molecules in pyrolysis oil and in water during hydrotreatment over nickel and ruthenium catalysts. *Biomass and Bioenergy* **106,** 63–73 (2017).

68. Khromova, S. A. *et al.* Anisole hydrodeoxygenation over Ni-Cu bimetallic catalysts: The effect of Ni/Cu ratio on selectivity. *Appl. Catal. A Gen.* **470,** 261–270 (2014).

69. Ardiyanti, A. R. *et al.* Catalytic hydrotreatment of fast pyrolysis oil using bimetallic Ni-Cu catalysts on various supports. *Appl. Catal. A Gen.* **449,** 121–130 (2012).

70. Yin, W. *et al.* Hydrotreatment of the carbohydrate-rich fraction of pyrolysis liquids using bimetallic Ni based catalyst: Catalyst activity and product property relations. *Fuel Process. Technol.* **169,** 258–268 (2018).

71. French, R. J. *et al.* Evaluate impact of catalyst type on oil yield and hydrogen consumption from mild hydrotreating. *Energy and Fuels* **28,** 3086–3095 (2014).

72. Zhang, X. *et al.* Characterization and catalytic properties of Ni and NiCu catalysts supported on ZrO 2 – SiO 2 for guaiacol hydrodeoxygenation. **33,** 15–19 (2013).

73. Reed, S. Introduction to Energy Dispersive X-ray Spectrometry. *Cent. Facil. Adv. Microsc. Microanal. Univ. California, Riverside* 1–12 (2018). doi:http://dx.doi.org/10.1590/S0104-66322011000100011

74. Hou, L., Bu, Q., Li, S., Wang, D. & Xie, T. Ni3S2-Decorated TiO2 nanotube arrays as effective photoanodes for photoelectrochemical water splitting. *RSC Adv.* **6,** 99081–99087 (2016).

75. Xiong, X. *et al.* One-step synthesis of architectural Ni3S2nanosheet-on-nanorods array for use as high-performance electrodes for supercapacitors. *NPG Asia Mater.* **8,** e300 (2016).